arXiv:1401.3085v1 [astro-ph.HE] 14 Jan 2014

16 Years of RXTE Monitoring of Five Anomalous X-ray Pulsars

Rim Dib[1] and Victoria M. Kaspi[2]
Department of Physics, McGill University, Montreal, QC H3A 2T8

ABSTRACT

We present a summary of the long-term evolution of various properties of the five non-transient Anomalous X-ray Pulsars (AXPs) 1E 1841−045, RXS J170849.0−400910, 1E 2259+586, 4U 0142+61, and 1E 1048.1−5937, regularly monitored with *RXTE* from 1996 to 2012. We focus on three properties of these sources: the evolution of the timing, pulsed flux, and pulse profile. We report several new timing anomalies and radiative events, including a putative anti-glitch seen in 1E 2259+586 in 2009, and a second epoch of very large spin-down rate fluctuations in 1E 1048.1−5937 following a large flux outburst. We compile the properties of the 11 glitches and 4 glitch candidates observed from these 5 AXPs between 1996 and 2012. Overall, these monitoring observations reveal several apparent patterns in the behavior of this sample of AXPs: large radiative changes in AXPs (including long-lived flux enhancements, short bursts, and pulse profile changes) are rare, occurring typically only every few years per source; large radiative changes are almost always accompanied by some form of timing anomaly, usually a spin-up glitch; only 20–30% of timing anomalies are accompanied by any form of radiative change. We find that AXP radiative behavior at the times of radiatively loud glitches is sufficiently similar to suggest common physical origins. The similarity in glitch properties when comparing radiatively loud and radiatively silent glitches in AXPs suggests a common physical origin in the stellar interior. Finally, the overall similarity of AXP and radio pulsar glitches suggests a common physical origin for both phenomena.

Subject headings: pulsars: individual (1E 1841−045) — pulsars: individual (RXS J170849.0−400910) — pulsars: individual (1E 2259+586), — pulsars: individual (4U 0142+61) — pulsars: individual (1E 1048.1−5937) — stars: neutron — X-rays: stars

1. Introduction

Prior to the 1995 December launch of NASA's *Rossi X-ray Timing Explorer (RXTE)*, there existed a major puzzle surrounding two apparently distinct class of high-energy sources, Soft Gamma Repeaters (SGRs) and Anomalous X-ray Pulsars (AXPs). At the time, three SGRs were known and were classified as such due to their distinctive repeating soft gamma-ray bursts. The famous 'March 5' event of 1979 (Mazets et al. 1979), involving SGR 0526−66 in the Large Magellanic Cloud and the release of over 10^{44} erg in just a few minutes, demonstrated the astonishing potential these objects have for explosive energy releases. The source of the energy for the bursts and this giant flare was unknown, but was proposed to be the decay of an enormous $> 10^{14} - 10^{15}$ G internal magnetic field in a young neutron star – the so-called "magnetar" model (Thompson & Duncan 1993; Thompson & Duncan 1995; Thompson & Duncan 1996).

Meanwhile, roughly half-a-dozen AXPs had been identified by van Paradijs et al. (1995) as 'anomalous' X-ray pulsars, spectrally distinct from conventional accreting pulsars, and lying all in the Galactic Plane, with one in a supernova remnant. Their spin-down luminosities failed by orders of magnitude to account for their apparently stable X-ray luminosities. For this rea-

[1]rim@physics.mcgill.ca
[2]vkaspi@physics.mcgill.ca

son, they were generally believed to be some strange form of low-mass X-ray binary, although no evidence for binary companions was seen (e.g. Mereghetti & Stella 1995; Baykal & Swank 1996; Baykal et al. 1998). Indeed the first *RXTE* observations of AXPs were done intending to search for Doppler shifts due to binary motion (Mereghetti et al. 1998). Thompson & Duncan (1996) however, noted some similarities between the AXPs and the SGRs, and suggested that both are magnetically powered isolated young neutron stars.

The post-*RXTE* picture of SGRs and AXPs has evolved considerably and indeed following intensive monitoring campaigns, such as that described in this paper, these objects appear no longer particularly 'anomalous', though certainly still remarkable. In particular, the discovery of X-ray pulsations in two SGRs during relatively quiescent phases, along with the direct measument of spin-down in those objects (Kouveliotou et al. 1998; Kouveliotou et al. 1999; Hurley et al. 1999), as quantitatively predicted in the magnetar model, provided compelling evidence that SGRs are indeed magnetars. Subsequently, the *RXTE* discovery of SGR-like bursts in two AXPs (Gavriil et al. 2002; Kaspi et al. 2003), consistent again with the expectations of the magnetar model as described by Thompson & Duncan (1996), argued strongly for the identification of both classes of objects as magnetars. The latter discovery was a result of a systematic AXP monitoring program that also demonstrated the great timing stability of some AXPs (Kaspi et al. 1999), that AXPs exhibit spin-up glitches (Kaspi et al. 2000), and a variety of other interesting AXP phenomenology that is generally understandable in the magnetar framework (Gavriil & Kaspi 2002; Dall'Osso et al. 2003; Woods et al. 2004; Gavriil et al. 2004; Gavriil & Kaspi 2004; Gavriil et al. 2006; Dib et al. 2007; Dib et al. 2008a, 2009a; Gavriil et al. 2011). While there are still some who argue that the quiescent X-ray emission of both classes is accretion-driven (e.g. Ertan et al. 2009; Alpar et al. 2011), practically all existing accretion models still demand magnetar-strength fields to power the observed bursts and giant flares. Regardless, the concensus today, based largely on *RXTE* observations like those reported on here, is that SGRs and AXPs are one in the same class of object, with the SGRs the more active of the family, but with clear transition objects between the two classes (e.g. Kaspi et al. 2001; Kulkarni et al. 2003; Israel et al. 2010). In other words, a continuum of behaviors between AXPs and SGRs has been observed such that their class definitions have been heavily blurred and the very names 'AXP' and 'SGR' seem synonymous. Nevertheless, in this paper we continue to refer to the targets as AXPs, mainly for consistency with past publications based on subsets of the data, but clearly noting that such nomenclature is somewhat out of date.

Much of today's understanding of AXPs in particular comes from the long-term systematic *RXTE* monitoring program of five AXPs. This program used short snapshot observations of the five bright, persistent AXPs taken regularly every few weeks in order to maintain full pulse phase coherence. This allowed the source's spin parameters to be measured with high precision, enabling sensitivity to glitches, and providing pulsed flux and pulse profile monitoring, in addition to sensitivity to bursting behavior. This paper presents a complete analysis of all *RXTE* data for the five AXP monitoring targets, which are listed along with their basic properties in Table 1. We present here a systematic and uniform analysis of data from the commencement of regular monitoring in 1998 (and even, in some cases, including data prior to that) and up to the final AXP observations made just before *RXTE* was shut off in early 2012. In total, we have analyzed 3202 individual *RXTE* observations of the targets, a total of 10 Ms taken over a span of 15.7 years. *RXTE* revealed many previous unknown AXP phenomena and answered many basic questions about AXPs and magnetars, but as this paper shows, it also raised many new questions that have significant bearing on our physical understanding of magnetars.

This paper is structured as follows. In §2, we present a quick overview of the five AXPs monitored in this project. In §3 we describe the *RXTE* observations of our targets. In §4 we summarize the three kinds of analysis performed: timing, pulsed flux, and pulse profile. In §5, we detail our results for each source. In §6, we consider the behavior of each source – as well as the collective behaviors of all the targets – and discuss our findings and their implications for the physical nature

of these objects.

2. Overview and Previous History of the Sources

2.1. 1E 1841−045

1E 1841−045 is a 7.8-s AXP located in supernova remnant Kes 73 (Vasisht & Gotthelf 1997). It was observed by *RXTE* roughly twice per month since 1999 February.

A study of a handful of archival X-ray observations of 1E 1841−045 spanning 15 years suggested the presence of deviations from a linear spin-down which were initially attributed to timing noise (Vasisht & Gotthelf 1997).

An analysis of the 1997−2006 *RXTE* monitoring observations of this source revealed that glitches had occured in 2002, 2003, and 2006 (Dib et al. 2008a). It also revealed a stable pulsed flux in the 2−20 keV band, and a stable pulse profile. Zhu & Kaspi (2010) showed that the phase-averaged flux was stable during the same period of time. A fourth glitch was reported by Dib et al. (2008b) and Dib et al. (2009b). The parameters for the 2nd glitch were revised by Dib et al. (2009b) and are restated in §5.1 of this work.

In 2010, 1E 1841−045 exhibited 4 episodes of short high-energy *Swift*-detected bursts. Bursts were detected on May 6 2010, 2011 February 9, 2011 June 23, and 2011 July 2 (Lin et al. 2011). The results of the analysis of the *RXTE* observations collected around the times of these bursts, as well as the remaining results of *RXTE* monitoring of 1E 1841−045, are presented in §5.1.

2.2. RXS J170849.0−400910

RXS J170849.0−400910 is an 11-s AXP discovered in 1996 (Sugizaki et al. 1997).

Like 1E 1841−045, RXS J170849.0−400910 glitches frequently. The first glitch detected from this source occured in 1999 (Kaspi et al. 2000), the second in 2001 (Kaspi & Gavriil 2003; Dall'Osso et al. 2003), and the third in 2005 (Dib et al. 2008a; Israel et al. 2007). Dib et al. (2008a) also reported on several glitch candidates, and reported no significant changes in the pulsed flux before 2006. These events were called 'glitch candidates' because a 4th or 5th order polynomial fit to the same data near glitch epochs resulted in similar timing residuals to those obtained from a glitch fit.

During the same time period as the *RXTE* monitoring, RXS J170849.0−400910 was observed sparsely with different X-ray imaging satellites *Chandra*, *XMM* and *Swift*. Rea et al. (2005), Campana et al. (2007) and Israel et al. (2007) analysed the imaging observations and reported the source's phase-average flux to be variable. Because the pulsed flux of the source was reported to be stable, this suggested an anti-correlation between the phase-averaged flux and the pulsed fraction. Rea et al. (2005), Campana et al. (2007) and Israel et al. (2007) also claimed a correlation between the flux variations and the glitches. This flux variation and correlation with glitches has recently been shown to have been spurious, however (Scholz et al., submitted.).

RXTE monitoring results for RXS J170849.0−400910 are presented in §5.2.

2.3. 1E 2259+586

1E 2259+586 is a 7-s AXP in the supernova remnant CTB 109 (Fahlman & Gregory 1981) and has been studied extensively. In particular Baykal & Swank (1996) reported fluctuations in the source's flux and spin down on a timescale of years. *RXTE* monitoring of 1E 2259+586 started in 1996.

After several years of stability, 1E 2259+586 entered an outburst phase in 2002 June in which almost every aspect of the emission suddenly changed: the pulsed and persistent flux, the pulsed fraction, the timing properties, the spectral properties, and the pulse profile (Kaspi et al. 2003; Woods et al. 2004). There is evidence that a similar event happened in 1990 (Iwasawa et al. 1992). The long-term recovery from the 2002 major outburst was studied by Zhu et al. (2008).

A second glitch occured in 2007 and was reported in Dib et al. (2008b), Dib et al. (2009b), Dib (2009), and Içdem et al. (2012). In contrast to the previous glitch, it was radiatively quiet. Içdem et al. (2012) also reported two timing anomalies, the second of which is discussed in §5.3 along with a summary of the results for this AXP. Very recently Archibald et al. (2013) reported on a sudden spin-down event, an 'anti-glitch,' as observed using *Swift* after our *RXTE*

monitoring ended.

2.4. 4U 0142+61

4U 0142+61 is an 8.7-s AXP. It was monitored with *RXTE* in 1997 and from 2000 to 2012. Morii et al. (2005) reported on a possible glitch having occured in 1999, in a data gap. Dib et al. (2007) showed that a glitch may have occured, but that a slow frequency increase cannot be ruled out. Dib et al. (2007) further showed that from 2000 to 2006, the source's pulsed flux rose by 29±8% in the 2−10 keV band. There were hints that the rise in the pulsed flux was towards the low-energy end of the band, which was consistent with the hints of spectral softening reported by Gonzalez et al. (2010) from the analysis of archival *XMM* data.

In 2006 March, 4U 0142+61 entered an active phase. It exhibited six X-ray bursts, as seen using *RXTE*, the last and largest of which was detected in 2007 February (Gavriil et al. 2011). During the active phase, the pulse morphology changed, then slowly recovered, and the frequency behaved as though it were recovering from a glitch, although the glitch parameters were difficult to determine because of the pulse profile changes. The pulsed flux underwent changes as well, but only for the duration of the observations containing the bursts. The results of the *RXTE* monitoring of 4U 0142+61 before, during, and after the active phase are presented in §5.4.

2.5. 1E 1048.1−5937

1E 1048.1−5937 is a 6.5-s AXP. It has a long history of timing variability and flux variability at many different wavebands (see for example, Mereghetti 1995, Mereghetti et al. 1998, and Paul et al. 2000).

1E 1048.1−5937 has been dubbed the "anomalous" Anomalous X-ray Pulsar because of its unique variability behavior. In 2001 and in 2002, the AXP exhibited two slow-rise pulsed flux flares, with a risetime on a timescale of weeks, and a decay on a timescale of months (Gavriil & Kaspi 2004). Gavriil et al. (2002) also reported two bursts from the direction of this source, which happened near the peak of the first pulsed flux flare. One of the two bursts was accompanied by a short-term pulsed flux enhancement. Two other bursts were detected from this source at later dates (Gavriil et al. 2006; Dib et al. 2009a).

Following the flares, in 2003, the pulsar underwent large (factor > 12) changes in its rotational frequency derivative on a timescale of weeks to months (Gavriil & Kaspi 2004), something never before seen in an AXP. It is unclear whether this timing-related episode and the preceding radiative flares are related. This was discussed further by Dib et al. (2009a).

Tiengo et al. (2005) reported on an *XMM* observation of 1E 1048.1−5937 in 2004, when the phase-averaged flux was lower than in 2003 but still not back to its 2000 value, and when the pulsed fraction was higher than in 2003 but still not back to its 2000 value, indicating that the source was still recovering from the second flare. They reported an anti-correlation between the total flux and the pulsed fraction.

Following the above events, from mid-2004 to 2007 March, 1E 1048.1−5937 went through a quiet phase. There was little variation in the spin-down, in the pulsed flux measured by *RXTE*, and in the total flux measured in a handful of X-ray imaging observations (Tam et al. 2008; Dib et al. 2009a).

In 2007 March, the source reactivated again (Tam et al. 2008; Dib et al. 2009a). The pulsed flux rose for the third time during the monitoring program, this time by a factor ~ 3 (2−10 keV), and the total flux rose by a factor of ~ 7 (2−10 keV). This was simultaneous with the largest AXP glitch observed by *RXTE* (see §5). A re-analysis of the *RXTE* data performed by Dib et al. (2009a) showed that the previous two flares observed from the source were also accompanied by timing events. Tam et al. (2008) analysed imaging observations from before and after the glitch and derived an anti-correlation between the pulsed fraction and the total flux. After the initial onset of the outburst, the timing and radiative parameters slowly recovered. A few months later, the source started experiencing rapid changes in the frequency derivative for the second time. An update on these variations is presented in §5.5 along with the remaining results of the 1E 1048.1−5937 *RXTE* monitoring.

3. Observations and Time Series Preparation

All observations presented here were obtained using the Proportional Counter Array (PCA) onboard *RXTE*. The PCA consisted of an array of five collimated xenon/methane multi-anode proportional counter units (PCUs) operating in the 2−60 keV range, with a total effective area of approximately 6500 cm^2 and a field of view of $\sim$1° FWHM (Jahoda et al. 1996).

Throughout the monitoring, we used the `GoodXenonwithPropane` and the `GoodXenon` data modes to observe our sources. Both data modes record photon arrival times with 1-μs resolution and bin photon energies into one of 256 channels. To maximize the signal-to-noise ratio, we analyzed only those events from the top Xenon layer of each PCU. The total number of *RXTE* observations analyzed for each source, as well as the dates of the first and the last analyzed observations, are shown in Table 2.

For each observation, we reduced the data to the solar system barycenter, and then extracted clean time series binned at a resolution of 1/32 s. For the timing and pulse profile analyses we extracted time series that included counts from all operational PCUs in a source-specific energy band that maximizes the signal-to-noise (see Table 2). For the pulsed flux analysis, we extracted time series in five bands (2−4 keV, 4−10 keV, 2−10 keV, 4−20 keV, and 2−20 keV), not including PCU 0 and PCU 1 because of the loss of their propane layers.

4. Analysis

4.1. Timing analysis

For the timing analysis, each barycentric binned time series was epoch-folded using an ephemeris determined iteratively by maintaining phase coherence as we describe below. When an ephemeris was not available, we folded the time series using a frequency obtained from a periodogram. Resulting pulse profiles, with 64 phase bins (32 bins in the case of 1E 1841−045), were cross-correlated in the Fourier domain with a high signal-to-noise template created by adding phase-aligned profiles. The cross-correlation returned an average pulse time-of-arrival (TOA) for each observation corresponding to a fixed pulse phase. To estimate the uncertainty on each TOA, we added to each folded profile many realizations of Poisson noise and re-cross-correlated each time. The phase uncertainty is determined from the standard deviation of the resulting simulated TOAs (Kaspi et al. 1999). The pulse phase ϕ at any time t can usually be expressed as a Taylor expansion,

$$\phi(t) = \phi_0(t_0)+\nu_0(t-t_0)+\frac{1}{2}\dot{\nu}_0(t-t_0)^2+\frac{1}{6}\ddot{\nu}_0(t-t_0)^3+\ldots, \quad (1)$$

where $\nu \equiv 1/P$ is the pulse frequency, $\dot{\nu} \equiv d\nu/dt$, etc., and subscript "0" denotes a parameter evaluated at the reference epoch $t = t_0$.

Once the TOAs were obtained, we performed two kinds of phase-coherent timing analyses on four of the AXPs (1E 1841−045, RXS J170849.0−400910, 1E 2259+586, and 4U 0142+61).

In the first type of timing analysis, we considered all stretches of time uninterrupted by timing discontinuities (see below). We fitted the TOAs in each time stretch to the above polynomial using the pulsar timing software package TEMPO[1]. TEMPO returned the best-fit polynomials coefficients, the phase-coherent timing solution, and also returned an absolute pulse number for each TOA. The resulting timing solutions are plotted as red lines in Panel a of Figures 1, 2, 3, and 4, and the corresponding timing residuals are shown in Panel c of the same Figures. Timing parameters from these fits are presented in Tables 3, 4, 5, and 6.

In the second type of timing analysis, we divided each inter-glitch (see below) stretch of time into many short overlapping segments. The number of TOAs contained in each segment depended on the cadence at which the source was observed. To get from one segment to the next, we shifted by one TOA. For each small segment, we fitted the TOAs to the above polynomial, allowing a single frequency derivative $\dot{\nu}$. The best-fit ν and $\dot{\nu}$ for all small segments are presented in Panels a and b of Figures 1 through 4. The horizontal error bars indicate the length of the individual segments, and the vertical error bars indicate the uncertainty in ν and $\dot{\nu}$.

[1]See http://www.atnf.csiro.au/research/pulsar/tempo.

Sudden changes in ν and $\dot{\nu}$ are called glitches. Slow variations in $\dot{\nu}$ are usually grouped under the name 'timing noise.' AXPs sometimes exhibit events in which it is difficult to determine whether a change in the timing properties occured abruptly or progressively over a short period of time. This often happens when the event occurs near a gap in the data. When the changes in the timing parameters at the epoch of such an event do not unambiguously identify it as a glitch, but are sufficiently abrupt (i.e., necessitating an ephemeris consisting of a polynomial of degree 4 or 5 to flatten the residuals near the epoch of the event), the discontinuities were called 'glitch candidates'. The timing parameters for the glitches and glitch candidates are presented in Table 7.

Since the spin-down of 1E 1048.1−5937 was particularly unstable, and phase coherence could only be maintained for periods of at most several months at a time (Kaspi et al. 2001; Gavriil & Kaspi 2004; Tam et al. 2008; Dib et al. 2009a), the timing analysis of 1E 1048.1−5937 was done differently. We broke the list of TOAs into many overlapping segments varying in length between 3 and 16 weeks depending on the local noise level of the source. For each segment we used TEMPO to fit the TOAs using Equation 1 and extracted absolute pulse numbers. We then checked that the pulse numbers of the observations present in overlapping segments were the same. This gave us confidence that the two overlapping ephemerides were consistent with each other and that phase coherence was not lost.

Combining all overlapping segments between two given dates yielded long time series of absolute pulse number versus TOA. The uncertainties on the TOAs were converted into fractional uncertainties in the pulse numbers. For 1E 1048.1−5937, because of irregularities in the spin-down, timing solutions spanning long periods of time required the use of very high-order polynomials, which tended to oscillate at the end points of fitted intervals. To eliminate the oscillations problem, instead of using these polynomials, we used splines. A spline is a piecewise polynomial function. It consists of polynomial pieces of degree n (here $n = 5$) defined between points called 'knots.' The two polynomial pieces adjacent to any knot share a common value and common derivative values at the knot, through the derivative of order $n-2$ (see Dierckx, 1975 for more details about splines). We fit a spline function through each pulse number time series, weighed by the inverse of the square of the fractional errors. To minimize oscillations in the spline due to noise, we set the spline smoothing parameter to allow the RMS phase residual obtained after subtracting the spline from the data points to be twice the average 1σ uncertainty in the pulse phase. The smoothing parameter controls the tradeoff between closeness and smoothness of fit by varying the polynomial coefficients and the spacing between the knots. We found the uncertainties on the spline by adding Gaussian noise to our data points 500 times, with mean equal to the 1σ uncertainty on each data point, fitting each time with a spline, averaging all the splines, and finding the standard deviation at each point.

The derivative of the spline function gave us the frequency of the pulsar as a function of time (Panel a of Fig. 5), and the second derivative of the spline gave us the frequency derivative of the pulsar (Panel b of Fig. 5). The corresponding timing residuals are shown in Panel 6 of the same Figure. A comparison of the timing residuals for the five AXPs is shown in Figure 6; see §5.2 for details.

For 1E 1841−045, we supplemented our *RXTE* timing data with two *XMM* observations taken on 2002 October 5 and 2002 October 7, made with the EPIC pn camera in large window mode. We made use of these data to help solve a phase ambiguity described in §5.1 below. These observations' OBSIDs are 0013340201 and 0013340101 and had integration times of 6.6 and 6.0 ks, repsectively. From these data, photons were extracted in a region of radius 32.5 arcseconds around the source, and photon arrival times were adjusted to the solar system barycenter. Then, from each observation, a time series in the 1.8−11 keV range with a time resolution of 47.7 ms was extracted, and a TOA was obtained from the time series using the method explained above.

4.2. Pulsed Flux Analysis

To determine the pulsed flux for each observation, we removed any bursts present in the time series, folded the data and extracted aligned pulse profiles in several energy bands. For each folded profile, we calculated the RMS pulsed flux,

$$F_{RMS} = \sqrt{2\sum_{k=1}^{n}((a_k{}^2 + b_k{}^2) - (\sigma_{a_k}{}^2 + \sigma_{b_k}{}^2))}, \quad (2)$$

where a_k is the $k^{\rm th}$ even Fourier component defined as $a_k = \frac{1}{N}\sum_{i=1}^{N} p_i \cos(2\pi ki/N)$, $\sigma_{a_k}{}^2$ is the variance of a_k, b_k is the odd $k^{\rm th}$ Fourier component defined as $b_k = \frac{1}{N}\sum_{i=1}^{N} p_i \sin(2\pi ki/N)$, $\sigma_{b_k}{}^2$ is the variance of b_k, i refers to the phase bin, N is the total number of phase bins, p_i is the count rate in the $i^{\rm th}$ phase bin of the pulse profile, and n is the maximum number of Fourier harmonics used. For each AXP, we made pulsed flux series with n=2 and n=6. For all AXPs, both series had the same behavior with slightly larger scatter when the larger number of harmonics was included. Some of the scatter may be due to low-level fluctuations in the pulse profile; see Panel e of Figures 1 through 5. The pulsed flux time series for each AXP is presented in Panel d of Figures 1 through 5.

4.3. Pulse Profile Analysis

For each observation, we folded the data in the same energy band used for timing using the best-fit frequency found in the timing analysis. We then cross-correlated the resulting profile with a standard template in order to obtain phase-aligned profiles. We used 32 phase bins for the aligned profiles. We then subtracted the respective averages from each of the aligned profiles and from the template. For each observation, we then found the scaling factor that minimized the reduced χ^2 of the difference between the scaled profile and the template. The resulting reduced χ^2 values are plotted in Panel e of Figures 1 through 5. These values are generally close to 1 except near the epochs of some major outbursts. For each AXP, the pulse profile for a typical observation, as well as the long-term average pulse profile, are shown in Figure 7.

4.4. Searching for Bursts

In addition to the timing, pulsed flux, and pulse profile analyses, we performed our burst-search routine introduced in Gavriil et al. (2002) and discussed further in Gavriil et al. (2004) on all the analysed observations. In short, for each data set, to determine whether a burst occured in the $i^{\rm th}$ time bin (of duration 31.25 ms in our analysis), the number of counts in that bin is compared to a local mean. The local mean is calculated over a stretch of four pulse periods of data, centered around the time bin being evaluated. A window of one pulse cycle is also administered so that counts directly from, and immediately around, the point under investigation would not contribute to the local mean. Bursts found by our searching procedure are presented in Table 8.

5. Results

5.1. 1E 1841−045

A summary of the behavior of 1E 1841−045 between 1996 and 2012 as seen by *RXTE* is shown in Figure 1. The long-term timing parameters of the source are presented in Table 3.

Panels a and b of Figure 1 reveal that 1E 1841−045 is a noisy source: the rotational frequency derivative varies significantly on a timescale of years. Panel c shows the residuals following the subtraction of our best-fit timing models, reported in Table 3.

1841−045 has exhibited four large glitches since the start of the monitoring program, marked by the vertical lines in Figure 1 (Dib et al. 2008a,b). Dib et al. (2008a) reported two possible sets of parameters for the first glitch from 1E 1841−045, with the most likely set involving an exponential recovery. However the addition of two TOAs extracted from *XMM* observations revealed the less likely timing solution to be the correct one (Dib et al. 2009b; Dib 2009).

There were no significant changes in the pulsed flux in any of the five studied bands near glitch epochs, nor were there any in glitch-free intervals. The 2−20 keV pulsed flux time series is shown in Panel d of Figure 1. Zhu & Kaspi (2010) showed that the source's phase-averaged flux is also stable, indicating that the glitches of 1E 1841−045 appear radiatively quiet.

In 2010 and 2011, *Swift* detected several episodes of bursts from 1E 1841−045, indicated by the four blue arrows pointing upward in the lower portion of Panel d of Figure 1. Lin et al. (2011) studied the bursting activity with *Swift* and *Fermi* and found that it did not have a significant effect on the persistent flux level of the

source. *RXTE* observations show that the pulsed flux of 1E 1841−045 appeared featureless around that time.

However, there were two hints in *RXTE* data indicating that the source was undergoing activity of some kind. First, there was a small burst (unresolved in a 31-ms time bin) observed from the direction of 1E 1841−045 on 2010 May 7, the day following the first episode of *Swift*-detected bursts (see Table 8). Note however that in the observation containing the burst, only a single PCU was on, making the pulse signal-to-noise ratio too low to allow verification of the presence of any fluctuations in the pulsed flux within that observation. Also note that in the *RXTE* observation collected on the previous day, there were no bursts.

The second indication that 1E 1841−045 was undergoing activity of some kind was a timing discontinuity (dotted line in Figure 1). The following is the sequence of events surrounding that discontinuity. From 2010 December 8 to 2011 January 16, there were no observations of the source made with *RXTE* because of the angular proximity of the source to the Sun. The first observation following the data gap was nominal, with no detected bursts, pulsed flux enhancement, or significant pulse profile changes. The second *Swift*-detected burst episode then occured on the February 8 and 9. This was followed again by two seemingly normal *RXTE* observations on February 9 and 10. However, the behavior of the timing residual around this time was peculiar: there was a change in the curvature of the timing residuals when a long-term polynomial timing solution fit included the stretch of time around the second burst episode, indicating a change in one or more timing parameters near that epoch. The change in the curvature of the residuals was not sufficiently abrupt to warrant calling the event a glitch candidate. Also, because of the presence of the gap in the data, it is difficult to determine whether the change in the timing parameters occured during the gap, between January 16 and February 10, or between February 10 and 23.

The peak in Panel b of Figure 1 that is indicated by the dotted vertical line provides another way of seeing the same phenomenon: each of the data points that are part of the rise and fall of the peak in Panel b include TOAs from before and after the data gap at the same time. Had there been no change in any of the timing parameters in or near the gap, this peak would not exist. However, because the data gap makes it impossible to constrain how fast and when the change in the timing parameters occured, and because the nearby TOAs can be fitted to an ephemeris consisting of a small number of frequency derivatives (here only three derivatives), we are not classifying the event as a glitch candidate. This event is reported in Table 7 as a notable timing discontinuity, along with the glitch parameters obtained from the most likely glitch epoch.

Panel e of Figure 1 shows no significant *RXTE*-detected pulse profile changes for this source. Note however that this Figure shows the reduced χ^2 statistics for individual pulse profiles, and although no significant changes are seen in this Figure, we believe there are constantly slow low-level changes, only detectable by summing the pulse profiles over an extended period of time; see for example Figure 11 of Dib et al. (2008a).

5.2. RXS J170849.0−400910

A summary plot of the behavior of RXS J170849.0−400910 between 1996 and 2012 as seen by *RXTE* is shown in Figure 2. The long-term timing parameters are presented in Table 4.

Panels a and b of Figure 2, show that RXS J170849.0−400910 underwent timing discontinuities: the solid lines mark the location of 3 glitches, one of which had an exponential recovery. Panel d shows that these glitches, like those of 1E 1841−045, showed no detectable pulsed flux variations; the exception to this being a single anomalous pulsed flux point in the 4−20 keV band in early 2010, far from the epochs of any timing discontinuities. We have studied this anomalous data point in detail but see no reason to distrust it. In addition to the glitches, there were many smaller-magnitude timing discontinuities, marked by the remaining vertical lines, and detected as peaks in Panel b.

Note that Israel et al. (2007) analysed a subset of these same data. In particular, they reported a glitch corresponding to our first glitch candidate, marked by the first dashed vertical line in Figure 2. For that event, the reported fit parameters are similar though not identical to ours (see Table 7). They also reported a glitch coincident with

the third solid vertical line of Figure 2. For that glitch, the reported frequency jump at the glitch epoch was similar to ours but the jump in frequency derivative was significantly different. We find that this difference is due to their inclusion of more post-glitch TOAs when fitting the glitch.

It is possible to compare the degree of abruptness of the changes in the timing parameters of J170849.0−400910 at the epochs of the various discontinuities by examining the peaks in Panel b of Figure 6. In this Figure, timing residuals of all AXPs are shown for selected stretches of time, after the removal of a long-term trend in frequency. The changes in the curvature of the residuals are, as expected, most abrupt at the location of the glitches. This Figure also provides a good way of visually comparing the amount of timing noise in the various sources by observing the number of "wiggles" in the timing residuals for a given number of frequency derivatives in the ephemeris used.

Panel e of Figure 2 shows no significant *RXTE*-detected pulse profile changes for this source. As for 1E 1841−045, however, we believe there could be constant slow low-level changes, only detectable by summing the pulse profiles over an extended period of time; see for example Figure 8 of Dib et al. (2008a).

5.3. 1E 2259+586

A summary of the behavior of 1E 2259+586 between 1997 and 2012 is presented in Figure 3. The long-term timing parameters of the source are presented in Table 5.

Panels a and b of Figure 3, and more clearly Panel c of Figure 6, show that 1E 2259+586 exhibits very little timing noise compared to the other AXPs. As shown by the solid vertical lines in Figure 3, 1E 2259+586 exhibited two glitches during our monitoring program.

The recovery of the first of the two glitches could be fit by a combination of exponentials (Kaspi et al. 2003; Woods et al. 2004). If the first post-glitch observation, which contained a large number of bursts, is excluded, the post-glitch data can also be fit with a simple ephemeris that includes one frequency derivative, followed by a long-term ephemeris that contains three frequency derivatives (red lines B1 and B2 in Panel a of Figure 3). This glitch was accompanied by a large enhancement in the pulsed flux (Panel d of Figure 3). The highest data point in this Panel is the average pulsed flux for the observation containing bursts. Note, however, that the pulsed flux during that observation fell monotonically with time; see Kaspi et al. (2003) and Woods et al. (2004) for details. The glitch was also accompanied by pulse profile changes (Panel e of Figure 3).

In contrast to the first glitch, the second glitch from this source was not followed by a recovery, and was radiatively quiet (Dib et al. 2008a,b, 2009b; Içdem et al. 2012).

Small but significant changes in the pulsed flux were again seen in two observations in 2009 January (Panel d of Figure 3) in all bands within the 2−20 keV range. The pulsar exhibited a pulse profile change during the first of these two observations (Panel e of Figure 3). One or more of the timing parameters changed within 50 days of the anomalous observation. (This can be most easily seen in Panel b of Figure 3 and in Panel c of Figure 6). The TOAs near this event can be fitted both to a sudden jump in frequency and to a polynomial with several frequency derivatives. Since the polynomial has only degree $n = 3$, the event is not classified as a glitch candidate, but is reported as a notable timing discontinuity in Table 7 because of the associated radiative changes. Moreover, it is also not classified as a glitch candidate because it is difficult to determine whether the change in the timing parameters occured slowly or abruptly. If abruptly, the epoch of the event can only be narrowed down to within a time period of 50 days.

This timing discontinuity is notable as when a glitch fit is attempted, independent of where the glitch epoch is chosen, the jump in frequency $\Delta\nu$ has a *negative* value between -1.00×10^{-8} and -1.42×10^{-8} Hz. This fact was remarked on in Içdem et al. (2012) as well, although they did not report the contemporaneous radiative changes, and their reported $\Delta\nu$ is 3.3-σ away from ours.

Finally, note that the anomalous χ^2 near MJD 50357 (Panel e of Figure 3) corresponds to the pulse profile of a very long observation, supporting the idea that there are constant low-level pulse profile changes that go undetected because of the low signal-to-noise ratio in most observations.

5.4. 4U 0142+61

A summary of the behavior of 4U 0142+61 between 1996 and 2012 as seen by *RXTE* is shown in Figure 4. The long-term timing parameters are presented in Table 6.

As can be seen from Figure 4, four noteworthy timing events occured during the X-ray monitoring of 4U 0142+61.

First, there is an offset in the frequency between the red lines representing ephemeris A and ephemeris B in Panel a of Figure 4. Based on the comparison of *RXTE* and *ASCA* data, Morii et al. (2005) pointed out that a glitch may have occured in the gap between the two ephemerides. The event is marked as a glitch candidate in Figure 4 and in Table 7.

The second interesting series of changes occured when the source entered an active phase in 2006 (second glitch candidate in Figure 4, timing parameters in Table 7). The pulsar's timing parameters changed, the pulse profile varied, and the pulsed flux increased locally within the three observations in which bursts were detected (arrows in Panel d). The details of this 2006 active phase of 4U 0142+61 were discussed by Gavriil et al. (2011). The timing event associated with this active phase is classified as a glitch candidate because the claim of a large sudden frequency jump is based on a single TOA, the first of the active phase, and that TOA may have been affected by pulse profile changes (Gavriil et al. 2011). If this TOA is omitted, the initial sudden spin-up is less significant, although it is clear that a change in $\dot{\nu}$ occured. Also, even if this TOA is omitted, extending the post-recovery ephemeris backward in time makes it look as though an 'anti-glitch' occurred (Gavriil et al. 2011).

Next occured a small and possibly slow timing discontinuity in 2009, most easily seen from Panel b of Figure 4 and from Panel d of Figure 6. This discontinuity is similar to the one exhibited by 1E 2259+586 in early 2009 (see §5.3) in that it can be fit both by a local polynomial of degree $n = 3$ in frequency and by a *negative* frequency jump of $1.3(2)\times10^{-8}$ Hz, very similar in size to that of the 1E 2259+586 event. However, unlike the 2009 discontinuity in 1E 2259+586, this event did not have contemporaneous radiative changes.

Finally, a large glitch occured in 2011 July. It was a radiatively silent glitch: there was at most a statistically marginal increase in the pulsed flux in all bands (see Fig. 4). Note that we chose the scale of Panel a of Figure 4 to show the data before and after this latest glitch, making the low-level changes in frequency due to timing noise hard to see. However, their presence is clear in Panel d of Figure 6.

5.5. 1E 1048.1−5937

A summary of the behavior of 1E 1048.1−5937 between 1997 and 2012 as seen by *RXTE* is shown in Figure 5. Long-term spin parameters are not presented in a Table like those of the other AXPs because of the very large timing noise of the source, necessitating multiple short-term ephemerides with a large number of frequency derivatives.

To visually appreciate the strength the timing noise of the source, refer to Panel e of Figure 6. The timing residuals for the period of time during which the pulsar was exhibiting the *least* timing noise are presented, after the subtraction of an ephemeris containing five frequency derivatives. Similar amplitude residuals with other AXPs can generally be obtained with only one or two frequency derivatives.

From a timing point of view, the period of time during which 1E 1048.1−5937 was observed by *RXTE* was very eventful (Panels a and b of Figure 5). First, from 1996 to 2001, the large timing noise and the sparsity of the data made it possible to only obtain phase-connected timing solutions for short (i.e. months-long) periods of time (Kaspi et al. 2001). In 2001, we adopted the strategy of observing the source in sets of three closely spaced observations, making phase connection easier.

The source exhibited two slow-rise pulsed flux flares (time scale weeks to months) in 2001 and 2002 (Panel d of Figure 5), previously reported by Gavriil & Kaspi (2004) and Gavriil et al. (2006). The flares were accompanied by variations in the frequency derivative (Panel b of Figure 5), although not as large or rapid as the dramatic changes of two orders of magnitude in the rotational frequency derivative which occured approximately a year later, starting in 2001 November (Panel b of Figure 5). The period of dramatic

frequency derivative changes lasted approximately 450 days, and was followed by a period of radiative quiescence during which there was significantly less timing noise (though still significantly more than in the other AXPs, see Figure 6).

On 2007 March 26, *RXTE* detected a large glitch from the source (see Table 7), and the pulsed flux started rising again (Panel d of Figure 5). Once again, less than a year after the pulsed flux started rising, another episode of large and rapid variations in the frequency derivative were observed.

Short bursts were observed on at least 4 occasions by *RXTE* (marked by arrows in Panel d of Figure 5), and on one other occasion where a large burst occured too close to the end of the observation, making it impossible to verify follow-up fluctuations in the pulsed flux within that observation. Deviations from the sinusoidal-looking pulse profile (see Figure 7) accompanied all three rises in the pulsed flux.

The last set of three consecutive *RXTE* observations of this source, taken on 2011 December 28, were anomalous: timing residuals were offset 0.15 in phase relative to the local ephemeris, and there was a hint of an increase in the pulsed flux. Fortunately subsequent *Swift* observations were made and in fact did confirm this was the start of a new event; these will be reported on elsewhere (Archibald et al. in prep.).

5.6. Glitch Table

This section contains the notes for Table 7.

- a. When the TOAs near a timing event can be fitted by a sudden jump in frequency as well as by an ephemeris consisting of 4 or 5 frequency derivatives, the event is labelled a "glitch candidate." When the TOAs near a timing event can be fitted by a sudden jump in frequency as well as by an ephemeris consisting of $\leq$3 frequency derivatives, the event is labelled a "notable timing discontinuity." Such discontinuities are more common, and only reported in this Table when they are associated with radiative changes.

- b. MJD range used for fitting the glitch. We fit for a single ν and $\dot{\nu}$ before the glitch and a sudden jump in ν and $\dot{\nu}$ at the time of the glitch. It is important to note that the value of the jump in $\dot{\nu}$ is very dependent on the amount of data used. We limited the period of time fitted, but included enough data to constrain $\dot{\nu}$.

- c. Total frequency jump at the glitch epoch.

- d. Total fractional frequency jump at the glitch epoch.

- e. For the glitches where no recovery was observed immediately after the glitch, this parameter represents the total jump in the frequency derivative at the glitch epoch. For the glitches with an exponential recovery, this represents the long-term change in the frequency derivative. This parameter is extremely sensitive to the amount of data included when doing the glitch fit, especially for noisy sources.

- f. Fraction Q of total $\Delta\nu$ recovered, and timescale of the exponential recovery, if any.

- g. Known radiative events associated with the glitch and observed with *RXTE*.

- h. Dib et al. (2008a) reported two possible sets of parameters for the first glitch from 1E 1841−045. Subsequently, with the help of two additional TOAs extracted from *XMM* data, we were able to constrain the fit parameters and show that the timing solution that we reported as least likely for that glitch (the one with the smaller frequency jump) was the correct one (Dib et al. 2009b; Dib 2009).

- i. See §5.1 for details.

- j. These two candidate glitches occurred in or near an observing gap. The frequency after the gap was higher than expected given the pre-gap ephemeris. Because the pre-gap and post-gap combined TOAs can be fit easily with a polynomial of degree 4 or 5, it is classified as a glitch candidate (Dib et al. 2008a).

- k. Israel et al. (2007) classified this event as a glitch.

- l. The difference between the value reported in Israel et al. (2007) and that reported in Dib et al. (2008a) can be attributed to the number of TOAs used when fitting for the glitch parameters.

- m. The difference between the sign of the value reported in Israel et al. (2007) and that reported in Dib et al. (2008a) can be attributed to the number of TOAs used when fitting for the glitch parameters.

- n. The model used to fit this glitch consists of a combination of rising and falling exponentials; see Woods et al. (2004) for details. The $\Delta\nu$ reported here is the maximum $\Delta\nu$ observed when comparing the pre-glitch and post-glitch frequencies.

- o. See §5.3 for details.

- p. Panel a of Figure 4 shows that a glitch might have occurred in the observing gap. The ranges of $\Delta\nu$ and of $\Delta\dot{\nu}$ reported here were obtained by extending the pre-gap ephemeris (consisting of a ν and a $\dot{\nu}$) forward, and the best-fit ephemeris of the two years after the gap (consisting of a frequency and a frequency derivative) backward to the gap boundaries.

- q. Morii et al. (2005) confined the glitch epoch to the 50893−51390 range of MJDs, where 50893 is the MJD for the last pre-gap *RXTE* observation of 4U 0142+61, and 51390 is the first inter-gap *ASCA* observation of the source.

- r. This is classified as a candidate glitch because the claim of a large sudden frequency jump is based on a single observation, the first of an active phase which the source entered in 2006. The TOA for that observation might be affected by pulse profile changes (Gavriil et al. 2011). If this TOA is omitted, the initial sudden spin-up is less significant, although it is clear that a change in $\dot{\nu}$ occured. Also, even if this TOA is omitted, extending the post-recovery ephemeris backward in time makes it look as though an 'anti-glitch' occurred (Gavriil et al. 2011). See §5.4 for details.

- s. The glitch marked the onset of an active phase in which there was a short-term (within individual observations) pulsed flux increase associated with the bursts (Gavriil et al. 2011). There also was a subtle 29±8% increase in the pulsed flux in the 2−10 keV band in the years preceding the active phase which might have been associated with the glitch (Dib et al. 2007; Gonzalez et al. 2010).

- t. See §5.4 for details.

- u. The timing noise in this source is always large compared to that of the other AXPs, most notably starting in 2002 November for a period of 450 days. Large variations in the rotational frequency derivative on timescales of weeks to months occured multiple times throughout the monitoring program, including ones that coincided with the onset of the two pulsed flux flares. We choose not to report these rapid changes as glitches as there would be too many. The timing noise was also particularly large at the onset of the two pulsed flux flares in late 2001 and early 2002, both of which were accompanied by timing anomalies of uncertain nature (Dib et al. 2009a). In this Table however, we are only reporting on the large glitch that occured in 2007, marking the end of a particularly quiet period (in timing and radiatively).

- v. There was a hint of a radiative and timing anomaly in the last set of three *RXTE* observations of 1E 1048.1−5937. However, the lack of follow-up *RXTE* monitoring observations made it impossible to determine whether a glitch, marking the end of another quiet period, occured at that time. Subsequent *Swift* observations confirm it was the start of a new event, and will be reported on elsewhere (Archibald et al., in prep.).

6. Discussion

We have reported on roughly 16 years and 10 Ms of regular, systematic *RXTE* monitoring of five AXPs on a weekly to monthly basis. This has yielded a rich and unique data set with which to examine magnetar rotational and radiative behavior. In particular, these data allow us to try

to identify common behavior and interesting differences from source to source. Indeed, what is clear is that each source has its own 'character', with no two of our targets behaving very similarly. For example, apart from well defined and highly localized timing anomalies, 1E 2259+586 is a very stable rotator, which contrasts strongly with 1E 1048.1−5937, which, even at its most stable, is still wildly erratic by comparison. That said, a systematic consideration of the data sets reveals some clear common behavior that can hopefully serve as a useful resource for developing a coherent theory to explain magnetar phenomenology.

Specifically, there are clear patterns in the radiative and timing anomalies in our targets. In Table 9, we present a concise summary of the different types of behaviors we have observed, in particular a 'scorecard' showing the fraction of observed anomalies that are accompanied by a different type of interesting behavior. In the Table, for each phenomenon listed in the far left column, we indicate in its row the fraction of times it is accompanied by the phenomenon listed at the top of each column. For example, of a total of 22 timing anomalies (including unambiguous glitches) observed in our full data set, 5 were accompanied by some form of flux change.

Several points are clear from examination of this Table:

(i) Radiative changes in our target AXPs are rare. In ∼16 yr of monitoring per source, we have detected only 5 long-lived episodes of flux variations, and only 6 cases of SGR-like bursting (where we define the 2002 outburst of 1E 2259+586 as a single case of bursting, in spite of there having been observed over 80 SGR-like bursts at one epoch). One caveat regarding this observation is that our *RXTE* monitoring was only sensitive to pulsed flux changes, whereas total flux changes can sometimes be larger (e.g. Tiengo et al. 2005). Our observations set the approximate time scale for radiative outbursts in AXPs at the several year level, at least for our sample. The latter is biased toward those sources that are brightest in quiesence; this inferred time scale may not apply to the so-called transient magnetars (e.g. Halpern & Gotthelf 2005). Also note we find evidence for constant low-level pulse profile and flux changes generically as discussed in §5, so though large radiative changes appear rare, at lower levels, they seem common.

(ii) Radiative changes are almost always accompanied by some form of timing anomaly. In all cases, flux enhancements and/or pulse profile changes were accompanied by some form of glitch or timing anomaly, and 5/6 burst episodes were similarly accompanied.

(iii) The converse of (ii) is not true: only occasionally (20-30% of the time) are timing anomalies in AXPs accompanied by any form of radiative anomaly. Equivalently, the large majority of AXP timing anomalies are radiatively silent, particularly but not uniquely in RXS J170849.0−400910 and 1E 1841−045, the two AXPs that glitch most often. This implicates the silent glitches as having an origin in the stellar interior, because if the rotational anomaly were due to physical changes in the magnetosphere, via enhanced currents for example, it seems likely that profile and/or flux changes should be present as well. Moreover magnetospheric current changes seem unlikely to produce abrupt spin-up events so similar to those seen in radio pulsars having far lower B fields (e.g. Espinoza et al. 2011; Yu et al. 2013).

Further, it is not necessarily the largest timing anomalies (i.e. the glitches with largest fractional frequency change) that are accompanied by radiative changes. Indeed using our strictest glitch definition, only 2 of 11 certain glitches had radiative changes. However, it seems possible that the greater the timing change, the greater the probability of there being a radiative change; for example, the largest glitch yet seen (see Table 7), in 1E 1048.1−5937, was accompanied by substantial radiative changes. Moreover there is no evidence that any other glitch property, such as recovery, is preferentially associated with radiative changes. Furthermore, the larger radiative outbursts do not necessarily correspond to the larger timing anomalies; for example the first of the two large flares in 1E 1048.1−5937 had only a small timing anomaly.

Note that there is significant overlap in properties of AXP glitches ($\Delta\nu$, $\Delta\dot{\nu}$) that do and do not have accompanying radiative behavior, and there are no particular timing differences between silent and loud timing events. These facts, together with the absence of obvious mechanisms to produce sudden radiatvely silent spin-ups in the magnetosphere, argue in favor of the hypothesis

that *all* AXP glitches have their physical origin in the stellar interior, as has long been hypothesized in radio pulsars (e.g. Anderson & Itoh 1975; Pines & Alpar 1985). Why some interior events produce radiative output while others do not could be related, for example, to the amount of energy released internally, or to the depth at which the event occurred.

(iv) When one type of radiative change occurs, usually multiple types of radiative changes occur. For example, pulse profile changes are, the large majority of the time, accompanied by a flux increase and SGR-like bursts. This clearly implicates external changes, though in our view these must accompany the internal events that caused the accompanying timing anomaly.

We note additionally that the apparently magnetar-like events observed in an otherwise conventional rotation-powered pulsar also conformed to the above trends. Specifically, in the 2006 magnetar-like outburst of the 0.326-s rotation-powered pulsar PSR J1846−0258 (Gavriil et al. 2008), the pulsar suffered a large rotational glitch in addition to SGR-like bursts and a large X-ray flux increase (but no apparent pulse profile changes). In this way, this event agreed with pattern (i), since such events are rare in this source, having occurred just once between 1999 and 2013, with (ii) because the radiative changes were accompanied by a timing anomaly, with (iii) because previously the source had glitched and showed no radiative changes (Livingstone et al. 2006), and with (iv) because both a flux change and SGR-like bursts occurred. Interestingly the only radiative anomalies yet to have been observed in the high-B radio pulsar PSR J1119−6127 were also at the time of a glitch (Weltevrede et al. 2011). All other radio pulsar glitches, were, as far as could be observed, radiatively silent, although prompt target-of-opportunity X-ray observations following glitches have not in general been done. The lone exception was for the 1999 spin-up glitch of the Vela pulsar, which was followed within a day by a *Chandra* X-ray observation that showed no change in flux (Helfand et al. 2001).

The majority of the magnetars presently known were discovered via SGR-like bursts, thanks to the existence of sensitive all-sky X-ray monitors such as the *Fermi* Gamma-Ray Burst Monitor and *Swift*'s Burst Alert Telescope (see Olausen & Kaspi 2013, and references therein). These sources, discovered in outburst, were not being monitored prior to discovery, so it is not known whether any form of timing anomaly accompanied the outburst. However, in some cases there are hints of glitch recovery post-outburst (e.g. Scholz et al. 2012), suggesting a glitch did occur. The results of our *RXTE* monitoring program suggest that all or nearly all magnetar outbursts are accompanied by timing anomalies; careful monitoring of sources in quiescence in case of future outbursts may be able to test this hypothesis.

Do the behaviors of the five sources we have monitored correlate with any of their inferred physical properties? There are hints of this, although with only five sources, all conclusions are tentative. Nevertheless we note that the source that is least stable and most prone to large radiative variations, 1E 1048.1−5937, is also the one with the highest quiescent blackbody temperature (0.56±0.01 keV), whereas the two most stable sources from a rotational point of view, 1E 2259+586 and 4U 0142+61, have the lowest quiescent temperatures (0.400±0.007 and $0.410^{+0.004}_{-0.002}$ keV, respectively), with the remaining two sources, 1RXS J1708−4009 and 1E 1841−045 having intermediate temperatures (0.456±0.009 keV and 0.45±0.03 keV, respectively), with all values as compiled by Olausen & Kaspi (2013) and based on spectral fitting using the phenomenological blackbody plus power-law models. We further note that 1E 2259+586 and 4U 0142+61, the two sources with the least amount of noise in their spin-down trend, have the lowest values of spin-inferred magnetic field strength (see Table 1), and 1RXS J1708−4009 and 1E 1841−045, the two sources that glitch most frequently, have the largest values. Thus, overall, our results suggest that higher-B sources and/or hotter sources show more timing activity. This is qualitatively as expected in the magnetar model since higher B implies stronger field decay, hence higher internal heating, greater interior stresses, and greater likelihood of crust cracking and magnetic structure changes (Thompson et al. 2002; Beloborodov 2009; Pons & Perna 2011; Perna & Pons 2011).

Dib et al. (2008a) calculated glitch activity parameters for the three AXP targets that had glitched in ∼8-9 yr of *RXTE* monitoring. They defined two different activity parameters: a_g was

the sum of the initial fractional frequency changes (including decaying components) divided by total observing span, and A_g was the same sum but in absolute value of the glitch (i.e. not fractional) again averaged over the span. We have recalculated these parameters for the same three sources as well as for the other two (both of which have now glitched) over the full *RXTE* span, where we take the absolute value of of the frequency changes for anti-glitches. Interestingly, we find a relatively narrow range of values for the five sources: $1.0 \times 10^{-14} < a_g < 3.3 \times 10^{-14}$ s^{-1}, and $1.5 \times 10^{-15} < A_g < 5.1 \times 10^{-15}$ Hz s^{-1}. Here the uncertainties are no larger than $\sim$10% of those values. This suggests that the magnetar glitch rate is roughly constant among sources, at least for the persistently bright AXPs that we have been monitoring. We note that the largest values of a_g and A_g in the above ranges come from 1E 1048.1−5937, 1E 1841−045 and RXS J1708−4009, the three with the largest inferred B values. This is consistent with our inference above that timing activity is correlated with that parameter. Comparing with activity parameters for radio pulsars compiled by Dib et al. (2008a), the above range of AXP values of a_g are comparable to those of the most actively glitching radio pulsars known, whereas the values of A_g are among those of the nearly most actively glitching pulsars known, but not quite as high as those of some sources. Dib et al. (2008a) also published histograms of glitch amplitude distributions for AXPs and radio pulsars; updating those results makes no qualitative difference to those histograms.

Apart from the above overall trends, several other behaviors we have observed are notable.

Archibald et al. (2013) recently reported a negative frequency step coincident with an X-ray outburst from 1E 2259+586 as observed using the *Swift* X-ray Telescope. They noted some previous possible anti-glitches, including one previously mentioned by Içdem et al. (2012) for this source. We have classified that event using our criteria as a timing anomaly; however as our pulsed flux analysis shows, the event was in fact coincident with a small X-ray flux enhancement (see Panel d in Fig. 3), as well as a brief, simultaneous change in the pulse profile (Panel e of Fig. 3). These radiative changes greatly support the hypothesis that an anti-glitch occured in early 2009 in this source given the Archibald et al. (2013) results, although we note that the magnitude of the spin-down in this earlier event is a factor of 4−9 smaller than in the *Swift* case, while the X-ray pulsed flux increased by an amount similar to that in the later event. The possible anti-glitch we report in 4U 0142+61 in early 2009 was not, however accompanied by any radiative changes, so we cannot confirm its veracity in that way. For 1E 2259+586, combining the *RXTE* and *Swift* events, the source has thus exhibited 2 spin-up and 2 spin-down glitches in 17 yr of monitoring; the equality of those numbers is striking, especially given the absence of any evidence for anti-glitches in 3 other AXPs we have monitored for comparable lengths of time, in spite of the detection of many spin-up events. Overall our results suggest that spin-down glitches in magnetars are much rarer than the spin-up variety. This is of course also true of radio pulsars, for which no spin-down glitches have been reported in spite of hundreds of spin-up glitches having been observed (e.g. Espinoza et al. 2011; Yu et al. 2013).

Additionally, in 1E 1048.1−5937, we have observed particularly unusual variations in spin-down rate in two events that are localized in time and both following relaxations from substantial pulse flux enhancements. Specifically, as previously reported by Gavriil & Kaspi (2004) and Dib et al. (2009a), order-of-magnitude torque variations lasting approximately one year were observed during the relaxations following the 2002 and 2007 flux flares, both during times of relative flux stability. The coincidental delay of the torque variations following the flares is suggestive of a causal relationship, however the lack of simultaneity of the two phenomena argue against accretion torque variations, since that predicts no such delay. Beloborodov (2009) discusses the possibility of delayed torque changes following a radiative outburst in magnetars, and suggests this is due to the delay in propagation of a disturbance in the field structure to the field-line bundle nearest the magnetic pole, where the torque originates. Why a single radiative outburst should result in the multiple torque variations seen is unclear in his picture however. We note that monitoring of this source using the *Swift* telescope, conducted after our *RXTE* observations ceased, has detected

a third such flux flare as well as a subsequent episode of torque variations. This is discussed in greater detail in an upcoming paper (Archibald et al., in prep.).

7. Conclusions

The long-term, systematic monitoring program of AXPs by *RXTE* has been valuable for illucidating the phenomenology of these unusual objects. With weekly to monthly data obtained over ∼16 yr for five objects, we have discovered a variety of phenomena, including outbursts and glitching, most of which strongly support the magnetar model. Here we have reported on repeated and remarkable large torque variations in 1E 1048.1−5937, curiously occuring months after large flux outbursts. We also report on a small pulsed flux and pulsed profile change at the time of a likely anti-glitch in 1E 2259+586. We have seen no radiative changes from 1RXS J1708−4009, and only apparent SGR-like bursts from 1E 1841−045 as far as radiative changes are concerned. 4U 0142+61 has shown a variety of low-level behaviors. All our targets have exhibited spin-up glitches at least once, and show differing levels of timing noise in inter-glitch intervals.

In this overall compilation of all the *RXTE* AXP monitoring data, we have noted the following patterns in AXP behavior: (i) large radiative changes of any kind in our sample are rare, occurring at most every several years; (ii) radiative changes in our AXPs are almost always accompanied by some form of timing anomaly, usually a spin-up glitch; (iii) the converse of (ii) is not true: only 20–30% of AXP timing anomalies are accompanied by any form of radiative change, with some evidence that the likelihood of such changes increases with glitch size; and (iv) when one type of radiative change occurs (e.g. flux outburst) there are usually others (e.g. pulse profile changes or bursts). There is an apparent tendency for the sources with higher spin-inferred magnetic fields and higher measured surface temperatures to be the most timing active, although the paucity of monitored sources makes this conclusion weak. The estimated glitch activities of all our targets are within a factor of ∼3–5 of each other (depending on precise definition), and are similar to those of the most actively glitching radio pulsars. Overall, the overlap in timing properties involved in spin-up and spin-down glitches seen thus far, together with the overlap of AXP glitch behavior compared with that seen in the radio pulsar population, is consistent with *all* glitching having origin in the stellar interior, and may be hinting at structural differences between high- and low-B neutron stars. On the other hand, the stellar magnetosphere may also play a role in the timing anomalies, especially in the radiative changes that sometimes accompany them.[2]

Although greatly illuminating of AXP behavior, these *RXTE* observations have raised many interesting questions that remain unanswered. Particularly noteworthy is the great diversity in our targets' behavior, which ranges from near-complete radiative stability over the 16-yr interval (1RXS J1708−4009 and 1E 1841−045) to large flux changes (1E 2259+586 and 1E 1048.1−5937). Moreover, the difference in timing stability from source to source is striking. Further, the subtle differences in glitch properties in AXPs compared to in radio pulsars is intriguing, and may be hinting at interesting structural differences. What role the magnetosphere may play in timing events remains to be seen. Continued systematic, long-term monitoring of these and other sources is a powerful way to help understand these objects, by better determining the statistics of glitches and radiative outbursts, and hopefully correlating them with physical properties of the sources in order to further constrain the physics of these remarkable objects.

We are grateful for the support we received over the years from the *RXTE* Guest Observers Facility, specifically Evan Smith and Divya Pereira for assistance with scheduling and particularly Jean Swank for her support of this project over so many years. We also thank Ed Morgan and Kenton Phillips for kindly permitting us and often assisting us in using MIT astrophysics computers and software for many years. We also acknowledge the

[2]Very recently, just prior to the submission of this paper, Lyutikov (2013; arXiv1306.2264) and Tong (2013; arXiv1306.2445) suggested that external mechanisms could explain the 1E 2259+586 anti-glitch reported by Archibald et al. (2013). However as we have argued here, we believe the systematic observations reported on here challenge those interpretations.

efforts of many people who have been involved in the *RXTE* monitoring project over the years: Deepto Chakrabarty, Fotis Gavriil, Eric Gotthelf, Jessica Lu, Julia Steinberger, and Pete Woods as well as Andrei Beloborodov, Andrew Cumming, Rob Duncan, Jeremy Heyl, Kostas Gourgouliatos, Maxim Lyutikov, Chris Thompson, and Dave Tsang for useful conversations at various times. VMK holds the Lorne Trottier Chair in Astrophysics and Cosmology, a Canada Research Chair, and is the R. Howard Webster Foundation Fellow of the Canadian Institute for Advanced Research (CIFAR). This work was supported in part by an NSERC Discovery Grant, the Centre de Recherche Astrophysique de Québec via FQRNT, a CIFAR Fellowship, a Killam Research Fellowship, and the NSERC John C. Polanyi Award.

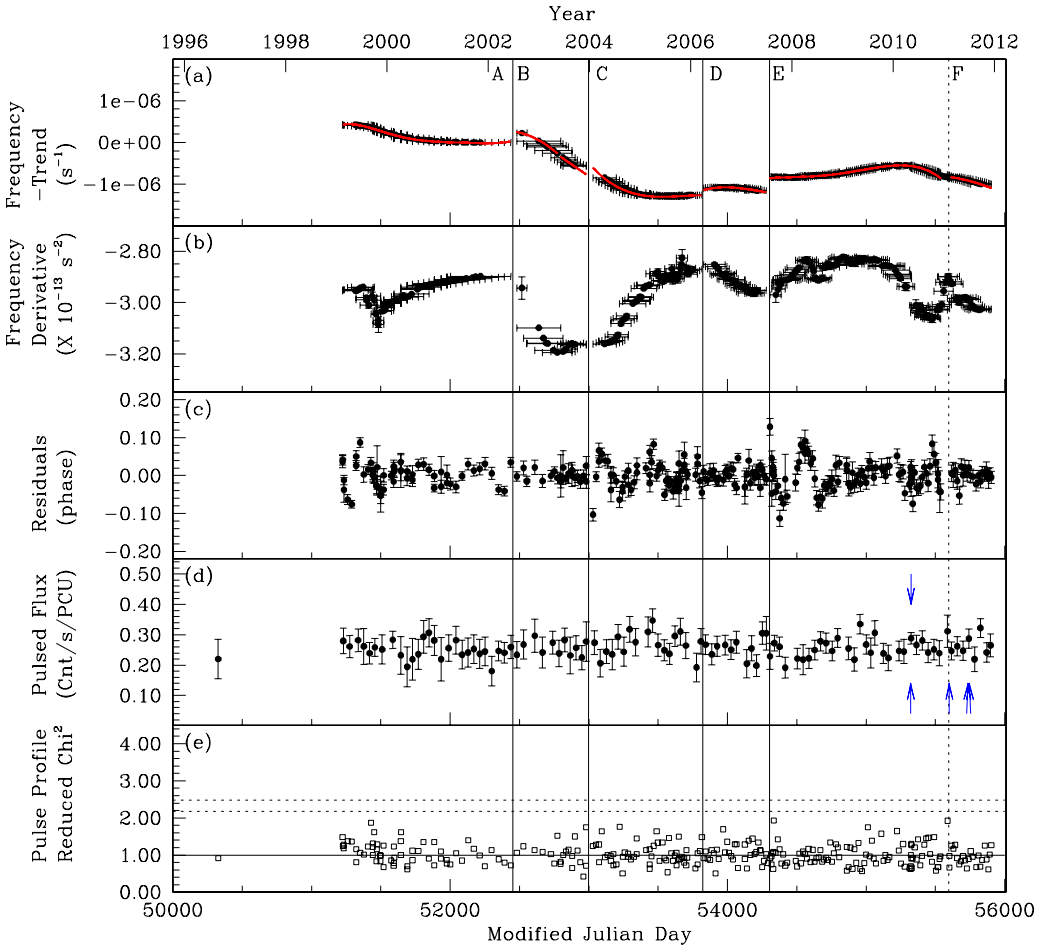

Fig. 1.— Long-term evolution of the properties of 1E 1841−045. (a) Frequency as a function of time with a linear trend in frequency subtracted. Red lines: long-term polynomial phase-coherent timing solutions. Polynomial start and stop times are at glitch epochs, candidate-glitch epochs, and epochs of other timing discontinuities. Data points: each data point corresponds to a frequency measurement obtained from a phase-coherent timing fit to a small number of TOAs (see §4.1 for details). (b) Frequency derivative as a function of time. Data points: each data point corresponds to a $\dot{\nu}$ measurement obtained from a phase-coherent timing fit to a small number of TOAs surrounding the epoch of the data point (see §4.1 for details). (c) Timing residuals corresponding to the red lines in the first Panel. (d) Pulsed flux in the 2−20 keV band, grouped in 30-day bins. The pulsed flux behaved similarly in all five analysed bands. The four blue arrows pointing upward indicate the location of the *Swift*-detected bursts (Lin et al. 2011). The blue arrow pointing down indicates the location of the *RXTE*-detected burst (see Table 8). (e) Reduced χ^2 statistics for the pulse profiles versus time, calculated after subtracting the scaled and aligned profiles of the individual observations from a high signal-to-noise template for 1E 1841−045. The solid horizontal line indicates a reduced χ^2 of 1. The lower dotted line corresponds to the 2σ significance level, after having taken the number of trials into account. The upper dotted line corresponds to the 3σ significance level. Vertical lines indicate timing discontinuities. Discontinuities marked by solid vertical lines are glitches and the dotted vertical line indicates the notable timing discontinuity (see Table 7).

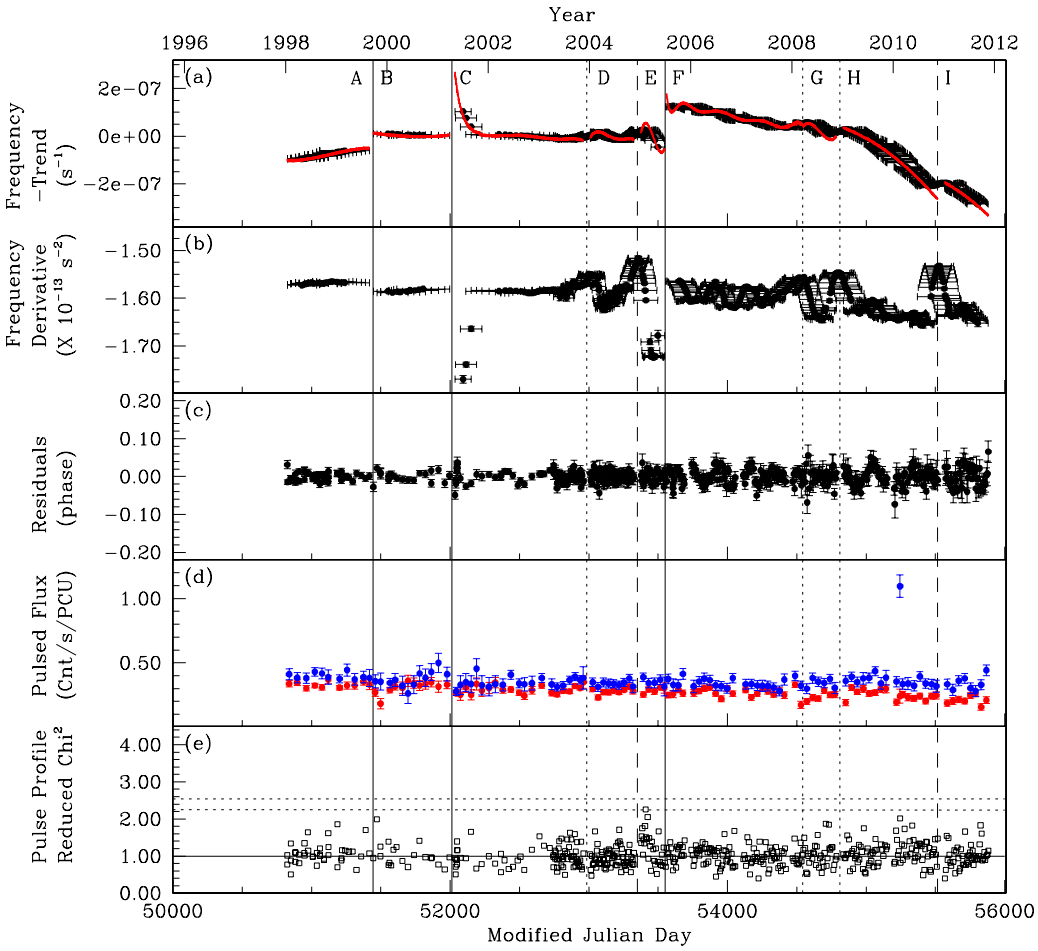

Fig. 2.— Long-term evolution of the properties of RXS J170849.0−400910. (a) Frequency as a function of time with a linear trend in frequency subtracted. Red lines: long-term polynomial phase-coherent timing solutions. Polynomial start and stop times are at glitch epochs, candidate-glitch epochs, and epochs of other timing discontinuities. Data points: each data point corresponds to a frequency measurement obtained from a phase-coherent timing fit to a small number of TOAs. (b) Frequency derivative as a function of time. Data points: each data point corresponds to a $\dot{\nu}$ measurement obtained from a phase-coherent timing fit to a small number of TOAs (see §4.1 for details). (c) Timing residuals corresponding to the red lines in the first Panel. (d) Pulsed flux in the 2−4 keV band (red points), and in the 4−20 keV band (blue points) grouped in 36-day bins. (e) Reduced χ^2 statistics for the pulse profiles versus time, calculated after subtracting the scaled and aligned profiles of the individual observations from a high signal-to-noise template for RXS J170849.0−400910. The solid horizontal line indicates a reduced χ^2 of 1. The lower dotted line corresponds to the 2σ significance level, after having taken the number of trials into account. The upper dotted line corresponds to the 3σ significance level. The solid vertical lines indicate the location of glitches, the dashed vertical lines indicate the locations of glitch candidates, and the dotted vertical lines indicate the location of other timing discontinuities (see Table 7).

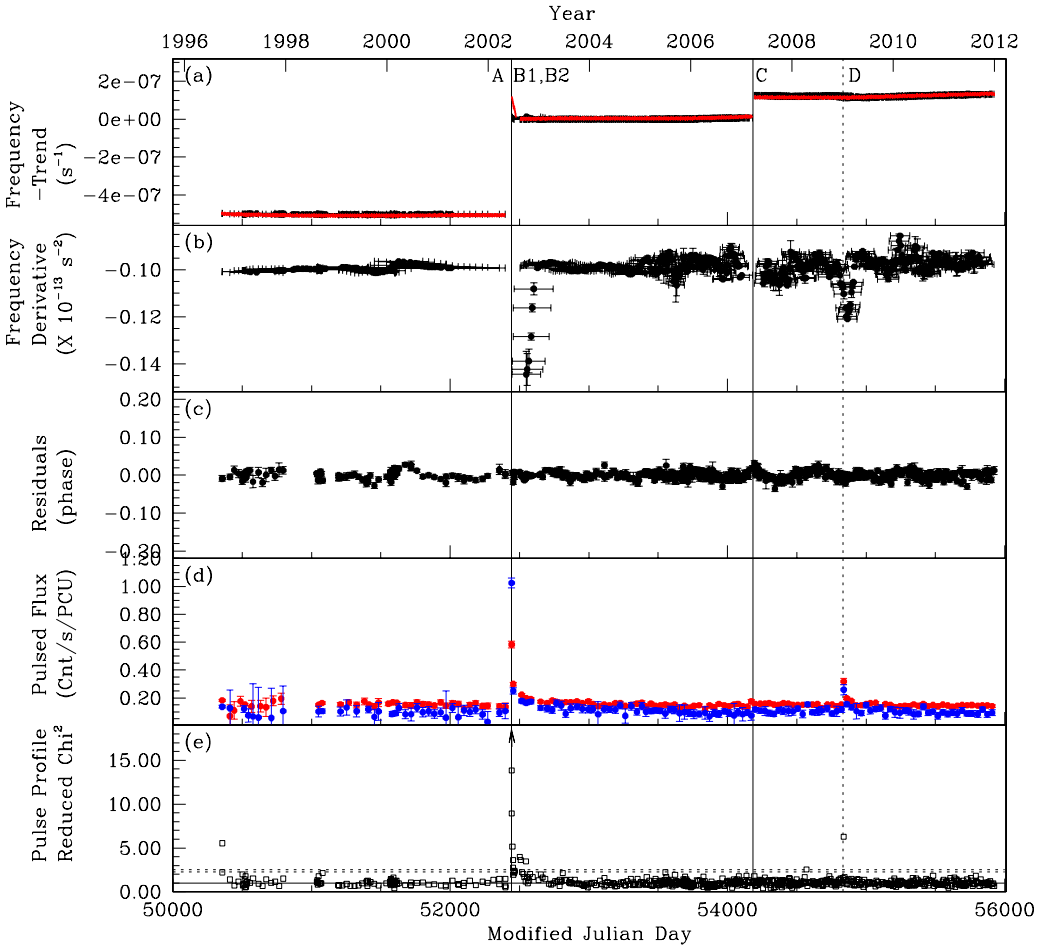

Fig. 3.— Long-term evolution of the properties of 1E 2259+586. (a) Frequency as a function of time with a linear trend in frequency subtracted. Red lines: long-term polynomial phase-coherent timing solutions. Red lines start and stop at glitch epochs, candidate-glitch epochs, and epochs of timing discontinuities. The B ephemeris is split into two segments. The first segment ends at the end of the recovery from the large 2002 glitch. Data points: each data point corresponds to a frequency measurement obtained from a phase-coherent timing fit to a small number of TOAs. (b) Frequency derivative as a function of time. Data points: each data point corresponds to a $\dot{\nu}$ measurement obtained from a phase-coherent timing fit to a small number of TOAs (see §4.1 for details) (c) Timing residuals corresponding to the red lines in the first Panel. (d) Pulsed flux in the 2−4 keV band (red points), and in the 4−20 keV band (blue points) grouped in 30-day bins. The first post-glitch observation in 2002 contained bursts (Gavriil et al. 2004). (e) Reduced χ^2 statistics for the pulse profiles versus time, calculated after subtracting the scaled and aligned profiles of the individual observations from a high signal-to-noise template for 1E 2259+586. The solid horizontal line indicates a reduced χ^2 of 1. The lower dotted line corresponds to the 2σ significance level, after having taken the number of trials into account. The upper dotted line corresponds to the 3σ significance level. The first post-glitch observation in 2002 is off the scale. The solid vertical lines indicate the location of glitches. The dotted vertical line indicates the location of a timing discontinuity; see §5.3 and Table 7 for details.

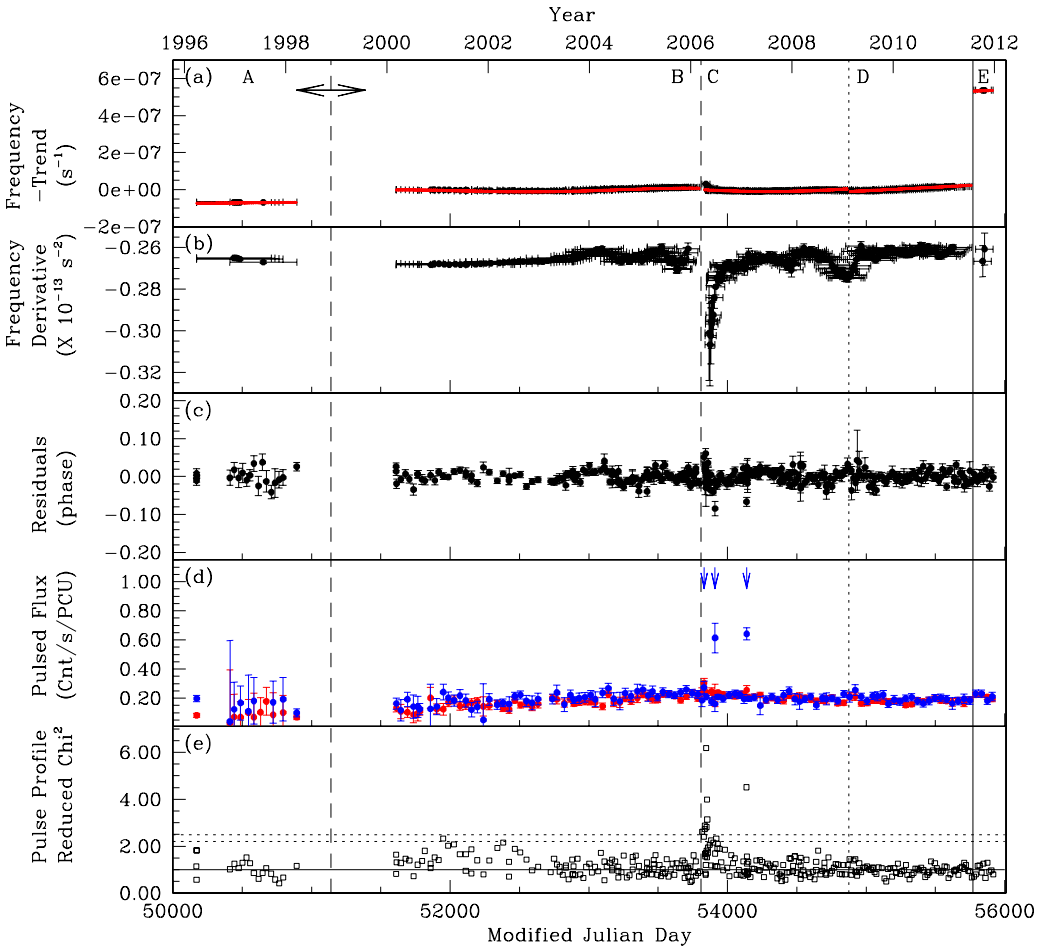

Fig. 4.— Long-term evolution of the properties of 4U 0142+61. (a) Frequency as a function of time with a linear trend in frequency subtracted. Red lines: long-term polynomial phase-coherent timing solutions. Polynomial start and stop times are at glitch epochs, candidate-glitch epochs, and epochs of timing discontinuities. Data points: each data point corresponds to a frequency measurement obtained from a phase-coherent timing fit to a small number of TOAs. The double-ended arrow indicates the time period during which the glitch candidate occured, as reported in Morii et al. (2005). (b) Frequency derivative as a function of time. Data points: each data point corresponds to a $\dot{\nu}$ measurement obtained from a phase-coherent timing fit to a small number of TOAs. (c) Timing residuals corresponding to the red lines in the first Panel. (d) Pulsed flux in the 2−4 keV band (red points), and in the 4−20 keV band (blue points) grouped in 30-day bins. The blue arrows indicate the locations of the *RXTE* observations containing bursts. (e) Reduced χ^2 statistics for the pulse profiles versus time, calculated after subtracting the scaled and aligned profiles of the individual observations from a high signal-to-noise template for 4U 0142+61. The solid horizontal line indicates a reduced χ^2 of 1. The lower dotted line corresponds to the 2 σ significance level, after having taken the number of trials into account. The upper dotted line corresponds to the 3 σ significance level. The solid vertical lines indicate locations of glitches. The dashed vertical lines indicate the locations of glitch candidates. The dotted vertical lines indicate locations of other timing discontinuities (see Table 7).

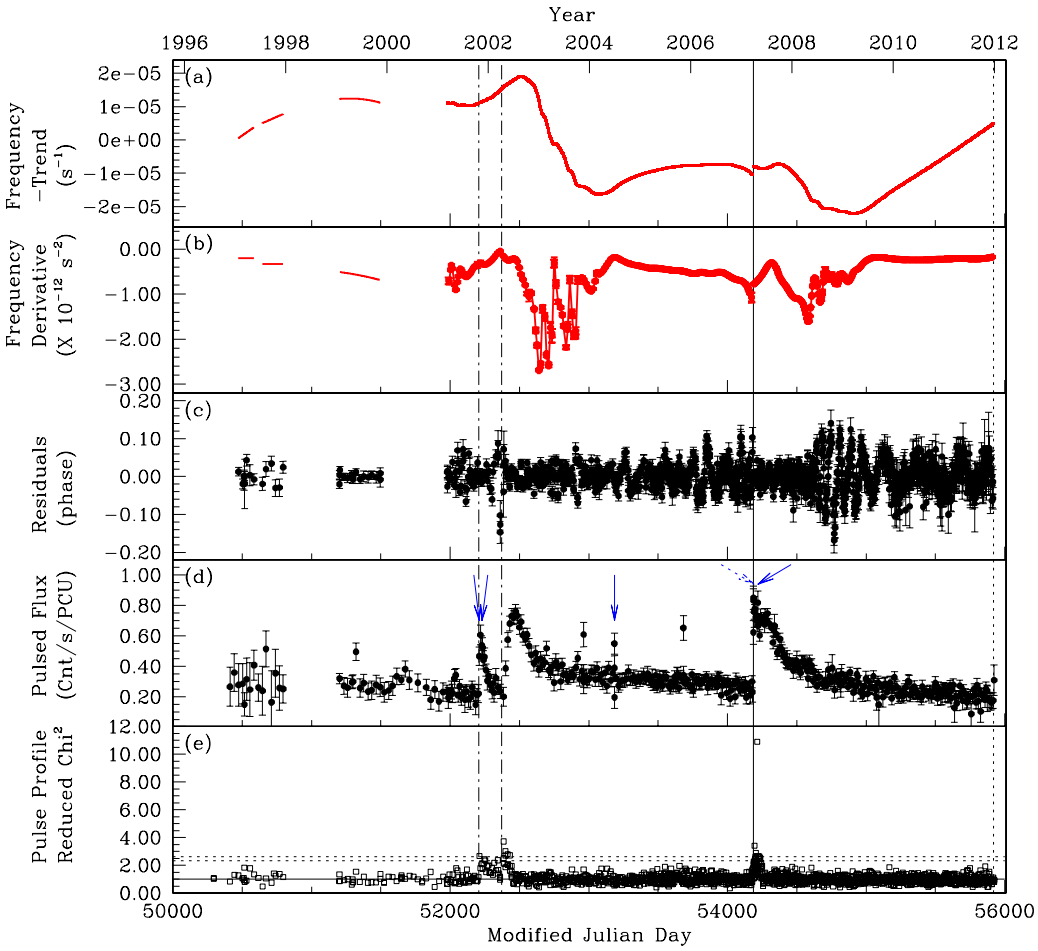

Fig. 5.— Long-term evolution of the properties of 1E 1048.1−5937. (a) Curves before the year 2000: ephemerides from Kaspi et al. (2001). Curve after the year 2000: frequency of 1E 1048.1−5937 as a function of time with a linear trend subtracted, obtained from spline fitting. (b) Curves before the year 2000: ephemerides from Kaspi et al. (2001). Curve after the year 2000: frequency derivative as a function of time, obtained from spline fitting. Data points: the spline evaluated at the epoch of the observations. (c) Timing residuals obtained after subtracting the TOAs from the ephemerides plotted in Panels a and b. (d) RMS pulsed flux in the 2−20 keV band binned every 7 days. The solid arrows mark the locations of the *RXTE*-detected bursts. The dotted arrow marks the location of a possible *RXTE*-detected burst. (e) Reduced χ^2 statistics for the pulse profiles versus time, calculated after subtracting the scaled and aligned profiles of the individual observations from a high signal-to-noise template for 1E 1048.1−5937. The solid horizontal line indicates a reduced χ^2 of 1. The lower dotted line corresponds to the 2σ significance level, after having taken the number of trials into account. The upper dotted line corresponds to the 3σ significance level. The dot-dashed vertical lines indicate the onset of the first two pulsed flux flares. The solid vertical line indicates the location of a glitch (see Table 7). The dotted line shown in 2012 is placed just before the last set of 3 *RXTE* observations of 1E 1048.1−5937, which were anomalous (see § 5.5).

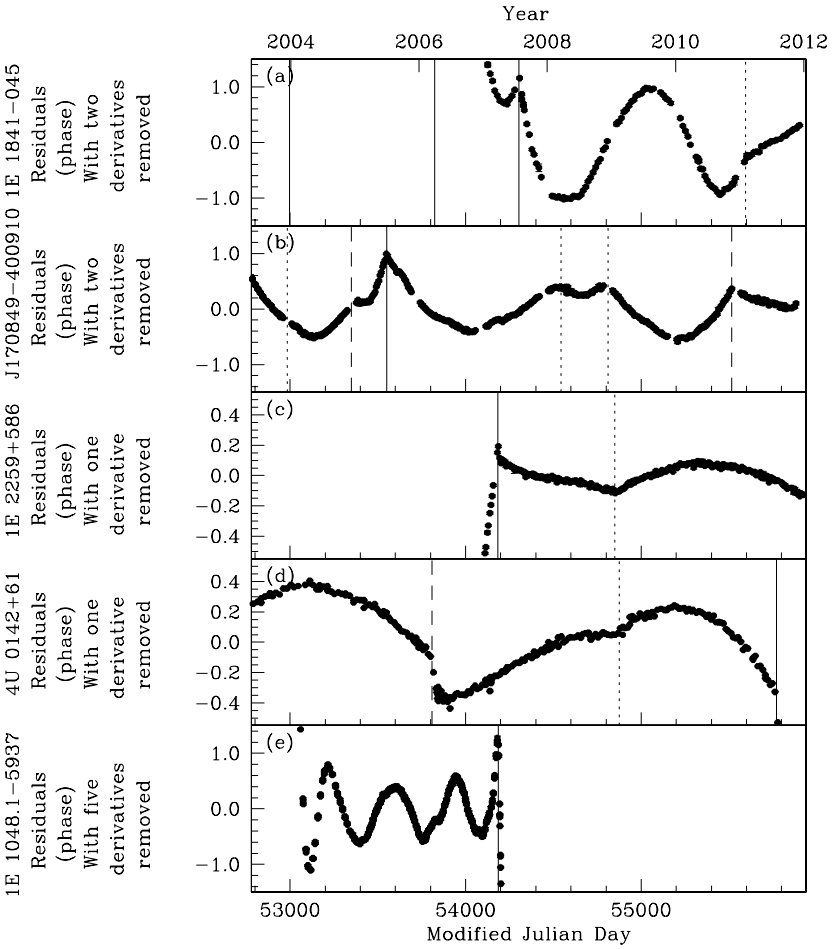

Fig. 6.— Timing residuals of the five AXPs for selected stretches of time. The residuals are obtained after subtracting the measured TOAs from those predicted by an ephemeris consisting of a frequency and of a small number of frequency derivatives. The number of derivatives was chosen in such a way as to avoid flattening the residuals, in order to show the changes in the curvature of the residuals caused by timing discontinuities. (a) Timing residuals for 1E 1841−045 corresponding to an ephemeris consisting of a ν, $\dot{\nu}$, and $\ddot{\nu}$ (a quadratic trend in frequency). (b) Timing residuals for RXS J170849.0−400910 corresponding to an ephemeris consisting of a quadratic trend in frequency. (c) Timing residuals for 1E 2259+586 corresponding to an ephemeris consisting of a linear trend in frequency. (d) Timing residuals for 4U 0142+61 corresponding to an ephemeris consisting of a linear trend in frequency. (e) Timing residuals for 1E 1048.1−5937 for the period of time when the AXP shows the least timing noise. The residuals correspond to an ephemeris consisting of the frequency ν and four frequency derivatives. Solid lines indicate glitches, dashed lines indicate glitch candidates, and dotted lines indicate other timing discontinuities.

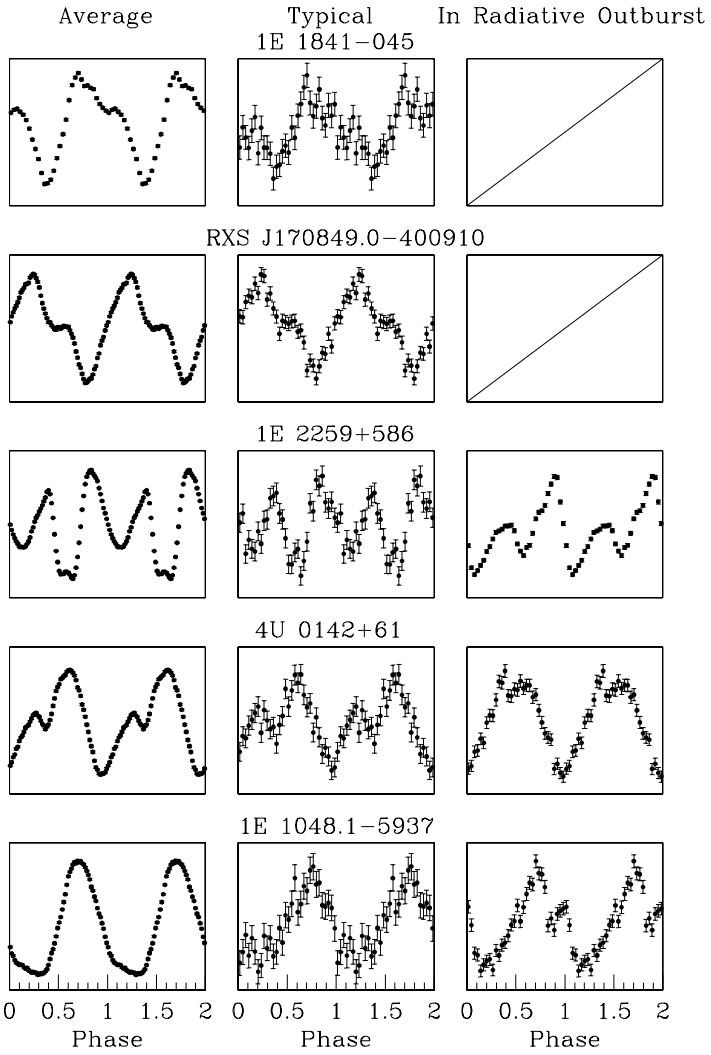

Fig. 7.— Pulse profiles from each of the five monitored AXPs in the following energy bands: 1E 1841−045: 2.0−11.0 keV, 1RXS J170849.0−400910: 2.0−5.5 keV, 1E 2259+586: 2.5−9.0 keV, 4U 0142+61: 2.5−9.0 keV, and 1E 1048.1−5937: 2.0−10.0 keV. *Left-Most Column:* the long-term average pulse profile. *Second Column:* pulse profiles from five typical observations, to show our usual data quality. *Right-Most Column:* pulse profiles of three AXPs in outburst. AXPs 1RXS J170849.0−400910 and 1E 1841−045 did not go into a radiative outburst while being monitored by *RXTE*. Note that the various plots in this Figure have different net integration times.

TABLE 1
SPIN PROPERTIES OF THE *RXTE*-MONITORED AXPS[a]

Parameter	1E 1841−045	RXS J170849.0−400910	1E 2259+586	4U 0142+61	1E 1048.1−5937
Period, P (s)	11.78	11.00	6.98	8.69	6.46
Frequency, $\nu \equiv 1/P$ (Hz)	0.085	0.091	0.143	0.115	0.155
$\dot{\nu}$ (10^{-13} Hz/s)[b]	−2.95	−1.60	−0.099	−0.268	−5.33
Magnetic Field[c] , B (G)	7.0×10^{14}	4.7×10^{14}	0.59×10^{14}	1.3×10^{14}	3.8×10^{14}

[a]For additional information on these sources see Olausen & Kaspi (2013) or the McGill Online Magnetar Catalog at http://www.physics.mcgill.ca/∼pulsar/magnetar/main.html.

[b]Estimate of the long-term value of $\dot{\nu}$ from ∼16 yr of *RXTE* monitoring.

[c]Magnetic fields calculated via $B \equiv 3.2 \times 10^{19}\sqrt{P\dot{P}}$ G.

Table 2

Summary of *RXTE* data analyzed for target AXPs

Source	Number of analysed PCA observations	Typical exposure per observation	Date of the first analysed observation	Date of the last analysed observation	Band used for the timing analysis
1E 1841−045	281[a]	5 ks	08/31/1996	12/08/2011	2−11 keV
RXS J170849.0−400910	522	2 ks	01/12/1998	11/17/2011	2−5.5 keV
1E 2259+586	608	5 ks	09/29/1996	12/29/2011	2.5−9 keV
4U 0142+61	339	5 ks	03/28/1996	12/22/2011	2.5−9 keV
1E 1048.1−5937	1452	2 ks	07/29/1996	12/29/2011	2−5.5 keV

[a]TOAs obtained from two *XMM* observations (2001 October 7 and 2002 October 5) were used to supplement those extracted from *RXTE* observations of 1E 1841−045; see §4.1 and 5.1 for details.

TABLE 3

LONG-TERM SPIN PARAMETERS FOR 1E 1841−045[a]

Parameter	Ephemeris A Spanning MJD 51225−52438	Ephemeris B1[b,c] Spanning MJD 52482−52774	Ephemeris B2[b] Spanning MJD 52610−52981	Ephemeris C Spanning MJD 53030−53816	Ephemeris D Spanning MJD 53829−54280	Ephemeris E Spanning MJD 54308−55538	Ephemeris F Spanning MJD 55616−55903
MJD start	51224.538	52481.594	52610.313	53030.093	53828.808	54307.465	55615.911
MJD end	52437.712	52773.487	52981.186	53815.842	54279.628	55538.066	55903.345
TOAs	56	9[b]	17	55	32	91	21
ν (Hz)	0.0849253010(8)	0.0848981884(13)	0.084888570(3)	0.084889876(6)	0.084868826(4)	0.084857001(4)	0.084824992(7)
$\dot{\nu}$ (10^{-13} Hz s^{-1})	−2.9954(7)	−3.158(6)	−3.179(2)	−3.340(7)	−2.834(5)	−2.866(6)	−2.944(11)
$\ddot{\nu}$ (10^{-22} Hz s^{-2})	3.13(11)	−10.1(9)	–	16.0(4)	−4.3(2)	−3.2(4)	−3.9(7)
$d^3\nu/dt^3$ (10^{-29} Hz s^{-3})	1.29(6)	–	–	−2.78(11)	–	2.86(17)	–
$d^4\nu/dt^4$ (10^{-36} Hz s^{-4})	−2.23(14)	–	–	–	–	−0.80(3)	–
$d^5\nu/dt^5$ (10^{-44} Hz s^{-5})	9.0(8)	–	–	–	–	–	–
Epoch (MJD)	51618.0001	52692.0000	53006.0000	53006.0000	53822.0000	54305.0000	55585.0000
RMS residual (phase)	0.031	0.014	0.028	0.036	0.024	0.041	0.017

[a]Numbers in parentheses are TEMPO-reported 1σ uncertainties.

[b]The B ephemeris was split into two segments because of the presence of a significant second frequency derivative for the first few months following the 2002 glitch.

[c]Including TOAs from two *XMM* observations.

Table 4

Long-Term Spin Parameters for RXS J170849.0−400910[a]

Parameter	Ephemeris A Spanning MJD 50826−51418	Ephemeris B Spanning MJD 51447−51996	Ephemeris C Spanning MJD 52036−52960	Ephemeris D Spanning MJD 53010−53325	Ephemeris E Spanning MJD 53377−53548	Ephemeris F Spanning MJD 53556−54541	Ephemeris G Spanning MJD 54548−54786	Ephemeris H Spanning MJD 54837−55517	Ephemeris I Spanning MJD 55568−55882
MJD start	50825.792	51446.610	52035.655	53010.094	53377.133	53555.734	54547.602	54836.798	55567.971
MJD end	51418.374	51995.679	52960.186	53325.061	53547.811	54540.671	54785.834	55516.933	55882.248
TOAs	39	20	74	69	29	124	34	84	45
ν (Hz)	0.090913817(3)	0.090906070(2)	0.090906067(11)	0.090892729(14)	0.09088760(2)	0.090885255(16)	0.090871541(12)	0.0908675842(14)	0.090857365(5)
$\dot{\nu}$ (10^{-13} Hz s^{-1})	−1.582(5)	−1.575(2)	−1.556(6)	−1.39(5)	−1.17(9)	−2.38(11)	−1.50(5)	−1.6064(11)	−1.618(8)
$\ddot{\nu}$ (10^{-22} Hz s^{-2})	−1.3(4)	3.2(8)	−8.1(1.8)	−45(11)	−138(25)	400(50)	−30(11)	−0.88(4)	−1.0(6)
$d^3\nu/dt^3$ (10^{-28} Hz s^{-3})	−0.050(12)	–	1.4(3)	5.5(1.6)	16(2)	−136(17)	3.0(1.0)	–	–
$d^4\nu/dt^4$ (10^{-35} Hz s^{-4})	–	–	−1.3(3)	−3.1(1.0)	–	343(44)	–	–	–
$d^5\nu/dt^5$ (10^{-43} Hz s^{-5})	–	–	6.9(1.5)	–	–	−6153(864)	–	–	–
$d^6\nu/dt^6$ (10^{-50} Hz s^{-6})	–	–	−1.7(4)	–	–	8494(1300)	–	–	–
$d^7\nu/dt^7$ (10^{-54} Hz s^{-7})	–	–	–	–	–	−8.6(1.5)	–	–	–
$d^8\nu/dt^8$ (10^{-61} Hz s^{-8})	–	–	–	–	–	6.1(1.1)	–	–	–
$d^9\nu/dt^9$ (10^{-68} Hz s^{-9})	–	–	–	–	–	−2.7(6)	–	–	–
$d^{10}\nu/dt^{10}$ (10^{-76} Hz s^{-10})	–	–	–	–	–	5.8(1.3)	–	–	–
$\Delta\nu_d$[b] (Hz)	–	–	$36(3)\times10^{-08}$	–	–	–	–	–	–
t_d[b] (days)	–	–	43(2)	–	–	–	–	–	–
Epoch (MJD)	51445.3846	52016.48413	52016.48413	52989.8475	53366.3150	53555.0000	54547.0000	54836.0000	55567.0000
RMS residual (phase)	0.011	0.012	0.015	0.013	0.016	0.019	0.022	0.022?	0.026

[a]Numbers in parentheses are TEMPO-reported 1σ uncertainties.

[b]Parameters held fixed at values determined from the glitch fit shown in Table 7.

TABLE 5

LONG-TERM SPIN PARAMETERS FOR 1E 2259+586[a]

Parameter	Ephemeris A Spanning MJD 50356−52398	Ephemeris B1[b] Spanning MJD 52445−52462	Ephemeris B2[b] Spanning MJD 52503−54181	Ephemeris C Spanning MJD 54194−54852	Ephemeris D Spanning MJD 54852−55924
MJD start	50355.891	52445.056	52503.050	54194.198	54852.303
MJD end	52398.421	52461.975	54180.566	54852.305	55924.287
TOAs	99	10	206	99	140
ν (Hz)	0.1432887919(2)	0.143287611(6)	0.1432874928(2)	0.14328612668(3)	0.14328554678(3)
$\dot{\nu}$ (10^{-14} Hz s^{-1})	−1.0201(17)	−4.8(7)	−0.9729(13)	−0.99307(13)	−0.96748(7)
$\ddot{\nu}$ (10^{-24} Hz s^{-2})	5.4(5)	–	−6.5(4)	–	–
$d^3\nu/dt^3$ (10^{-31} Hz s^{-3})	−0.43(7)	–	1.05(5)	–	–
Epoch (MJD)	50355.0000	52445.0000	52445.0000	54187.0000	54852.0000
RMS residual (phase)	0.016	0.0077	0.0087	0.012	0.010

[a]Numbers in parentheses are TEMPO-reported 1σ uncertainties.

[b]The B ephemeris is split into two segments. The first segment excludes the observation containing bursts, and stops at the end of the recovery of the pulsar from a large glitch.

TABLE 6

LONG-TERM SPIN PARAMETERS FOR 4U 0142+61[a]

Parameter	Ephemeris A Spanning MJD 50171−50893	Ephemeris B Spanning MJD 51611−53800	Ephemeris C Spanning MJD 53831−54867	Ephemeris D Spanning MJD 54881−55763	Ephemeris E Spanning MJD 55778−55917
MJD start	50170.693	51610.636	53831.335	54881.291	55777.699
MJD end	50893.288	53800.134	54867.298	55762.825	55917.361
TOAs	19	118	116	70	11
ν (Hz)	0.115096868(3)	0.1150921156(7)	0.1150921068(7)	0.1150920514(11)	0.115088121(5)
$\dot{\nu}$ (10^{-14} Hz s^{-1})	−2.659(3)	−2.679(5)	−2.714(4)	−2.621(8)	−2.64(6)
$\ddot{\nu}$ (10^{-23} Hz s^{-2})	–	−2.0(2)	1.14(8)	–	–
$d^3\nu/dt^3$ (10^{-31} Hz s^{-3})	–	−5.5(5)	–	–	–
$d^4\nu/dt^4$ (10^{-39} Hz s^{-4})	–	−5.5(5)	–	–	–
Epoch (MJD)	51704.000025	53800.0000	53800.0000	53800.0000	55762.0000
RMS residual (phase)	0.019	0.015	0.021	0.016	0.012

[a]Numbers in parentheses are TEMPO-reported 1σ uncertainties.

Table 7

Glitches Observed in the Monitored Anomalous X-ray Pulsars*,†

Glitch Number[a]	MJD Range[b]	Glitch Epoch (MJD)	$\Delta\nu$[c] (Hz)	$\Delta\nu/\nu$[d]	$\Delta\dot{\nu}$[e] (Hz/s)	Q[f] of Recovery	τ[f] of Recovery (days)	Associated Radiative Events[g]	References
1E 1841−045									
Glitch 1[h]	52300−52610	52453.132194	$2.91(10)\times10^{-7}$	$3.43(12)\times10^{-6}$	$-1.28(12)\times10^{-14}$	—	—	—	Dib et al. (2008a) Dib et al. (2009b) Dib (2009)
Glitch 2	52773−53244	52997.049200	$2.08(4)\times10^{-7}$	$2.45(4)\times10^{-6}$	$+4(3)\times10^{-16}$	—	—	—	Dib et al. (2008a)
Glitch 3	53579−53971	53823.969400	$1.17(7)\times10^{-7}$	$1.38(9)\times10^{-6}$	$+2(1)\times10^{-15}$	—	—	—	Dib et al. (2008a)
Glitch 4	54209−54348	54304.150312	$4.6(3)\times10^{-7}$	$5.5(4)\times10^{-6}$	$-2.1(1.4)\times10^{-14}$	—	—	—	Dib et al. (2008b) Dib et al. (2009b) Dib (2009)
Notable Timing Discontinuity[i]	55363−55728	55596.958500	$8.2(7)\times10^{-8}$	$8.2(7)\times10^{-8}$	$+4.4(1.2)\times10^{-15}$	—	—	*Swift*, *Fermi* & *RXTE* detected bursts within a few days	This paper
RXS J170849.0−400910									
Glitch 1	51186−51614	51445.384600	$5.1(3)\times10^{-8}$	$5.6(3)\times10^{-7}$	$-8(4)\times10^{-16}$	—	—	—	Kaspi et al. (2000) Dib et al. (2008a)
Glitch 2	51614−52366	52016.484130	$2.2(4)\times10^{-8}$ (long-term) $+3.6(3)\times10^{-7}$ (recovered)	$4.2(2)\times10^{-6}$	$-1.1(2)\times10^{-15}$	0.94(11)	43(2)	Possible profile changes	Kaspi & Gavriil (2003) Dall'Osso et al. (2003) Dib et al. (2008a)
Candidate-glitch 1[j,k]	53229−53456	53366.315000	$5.5(8)\times10^{-8}$	$6.0(8)\times10^{-7}$	$-1.9(1.3)\times10^{-15}$[l]	—	—	Possible profile changes	Dib et al. (2008a) Israel et al. (2007)
Glitch 3	53465−53631	53549.150950	$2.46(9)\times10^{-7}$	$2.71(10)\times10^{-6}$	$-2(2)\times10^{-15}$[m]	—	—	—	Dib et al. (2008a) Israel et al. (2007)
Candidate-glitch 2[j]	55315−55755	55517.1247	$9.4(5)\times10^{-8}$	$1.03(5)\times10^{-6}$	$+1.4(4)\times10^{-15}$	—	—	—	This paper
1E 2259+586									
Glitch 1[n]	51623−52900	52443.130000	$\sim4.95\times10^{-7}$ (long-term) + $\sim1.12\times10^{-7}$ (recovered)	$4.24(11)\times10^{-6}$	$+2.18(25)\times10^{-16}$	0.185(10)	12−17	Bursts, pulsed and total flux enhancements, large profile changes	Woods et al. (2004) Kaspi et al. (2003)
Glitch 2	54085−54256	54184.903200	$1.261(4)\times10^{-7}$	$8.80(3)\times10^{-7}$	$-6(2)\times10^{-16}$	—	—	—	Dib et al. (2008a) Dib et al. (2008b) Dib et al. (2009b) Dib (2009) Içdem et al. (2012)
Notable Timing Discontinuity[o]	54571−55112	54832−54880[o]	$-1.2(3)\times10^{-8}$[o]	$-8.2(2.1)\times10^{-8}$	$+2.3(1.6)\times10^{-16}$	—	—	Profile change in 1 obs. Pulsed flux and count rate change in 2 obs.	Içdem et al. (2012) This paper
4U 0142+61									
Candidate-glitch 1[p]	50170−52340	50893−51610[q]	(6.7(3)−8.1(3))$\times10^{-8}$	(5.8(2)-7.0(2))$\times10^{-7}$	$-2.4(3)\times10^{-16}$	—	—	Possible profile changes	Morii et al. (2005) Dib et al. (2007)
Candidate-glitch 2[r]	53481−54235	53809.185840	$-1.27(17)\times10^{-8}$ (long-term) $+2.0(4)\times10^{-7}$ (recovered)	$1.6(4)\times10^{-6}$	$-3.1(1.2)\times10^{-16}$	1.0(3)	17.0(1.7)	Bursts, short-term pulsed flux increase[s], pulse profile changes	Gavriil et al. (2011)
Glitch 1[t]	55329−55917	55771.190600	$5.11(4)\times10^{-7}$	$4.44(4)\times10^{-6}$	0[t]	—	—	Hint of a pulsed flux increase (1σ level)	This paper
1E 1048.1−5937									
Glitch 1[u,v]	54164−54202	54185.912956	$2.52(3)\times10^{-6}$	$1.63(2)\times10^{-5}$	$-6(4)\times10^{-14}$	—	—	Onset of third pulsed (and total) flux flare, some profile changes	Dib et al. (2009a) Dib et al. (2008b) Tam et al. (2008)

* Numbers in parentheses are TEMP(

See §5.6 for the text of the tablenotes “a” to “v”.

TABLE 8
RXTE-DETECTED BURSTS

Source	Date	Observation Containing Bursts	Number of Bursts Detected	Reference	Associated With
1E 1841−045	07/05/2010	95017-03-01-00	1	This paper	The 2010 May period of bursting activity, as observed by *Swift* and *Fermi*, (Lin et al. 2011).
RXS J170849.0−400910	–	–	–	–	–
1E 2259+586	18/06/2002	70094-01-03-00	>80	Gavriil et al. (2004) Kaspi et al. (2003) Woods et al. (2004)	The 2002 July major outburst.
4U 0142+61	06/04/2006	92006-05-03-00	1	Gavriil et al. (2011)	The 2006−2007 active phase.
	25/06/2006	92006-05-09-01	4	Gavriil et al. (2011)	The 2006−2007 active phase.
	07/02/2007	92006-05-25-00	1	Gavriil et al. (2011)	The 2006−2007 active phase.
1E 1048.1−5937	29/10/2001	60069-03-35-00	1	Gavriil et al. (2002) Gavriil & Kaspi (2004)	The first of two slow-rise flares.
	14/11/2001	60069-03-37-00	1	Gavriil et al. (2002) Gavriil & Kaspi (2004)	The first of two slow-rise flares.
	29/06/2004	90076-02-09-02	1	Gavriil et al. (2006)	–
	04/04/2007	92005-02-01-00	Possibly 1	This paper	The 2007 outburst.
	28/04/2007	92005-02-08-01	1	Dib et al. (2009a)	The 2007 outburst.

Table 9

Summary of *RXTE*-observed AXP Notable Event Phenomenology

Phenomenon	Accompanying Glitch/Anomaly[a]	Accompanying Flux Increase[b]	Accompanying Profile Change[c]	Accompanying X-ray Bursts[d]
Glitch/Anomaly[a]	...	5/22	6/22	5/22
Flux Increase[b]	5/5	...	5/5	4/5
Profile Change[c]	6/6	5/6	...	5/6
X-ray Bursts[d]	5/6	4/6	5/6	...

[a]The number of any form of *RXTE*-observed timing anomaly including glitches, and excluding the early 2012 event for AXP 1E 1048.1−5937, which occured within days of our last observation.

[b]The number of *RXTE*-observed long-lived episodes of pulsed flux variations, excluding the small hint of pulsed flux increase in AXP 4U 0142+61 following its 2011 glitch.

[c]The number of *RXTE*-observed pulse profile changes, excluding the two possible pulse profile changes following timing anomalies in AXP RXS J170849.0−400910.

[d]The number of *RXTE*-observed X-ray burst events. When a timing anomaly or a slow radiative event were followed by several bursts, the collection of bursts counts as one burst event.

REFERENCES

Alpar, M. A., Ertan, Ü., & Çalışkan, Ş. 2011, ApJ, 732, L4

Anderson, P. W. & Itoh, N. 1975, Nature, 256, 25

Archibald, R. F., Kaspi, V. M., Ng, C.-Y., Gourgouliatos, K. N., Tsang, D., Scholz, P., Beardmore, A. P., Gehrels, N., & Kennea, J. 2013, nat, submitted

Archibald, R. F., Kaspi, V. M., Ng, C.-Y., Gourgouliatos, K. N., Tsang, D., Scholz, P., Beardmore, A. P., Gehrels, N., & Kennea, J. A. 2013, Nature, 497, 591

Baykal, A. & Swank, J. 1996, ApJ, 460, 470

Baykal, A., Swank, J. H., Strohmayer, T., & Stark, M. J. 1998, A&A, 336, 173

Beloborodov, A. M. 2009, ApJ, 703, 1044

Campana, S., Rea, N., Israel, G. L., Turolla, R., & Zane, S. 2007, A&A, 463, 1047

Dall'Osso, S., Israel, G. L., Stella, L., Possenti, A., & Perozzi, E. 2003, ApJ, 599, 485

Dib, R. 2009, PhD thesis, McGill University, Canada

Dib, R., Kaspi, V. M., & Gavriil, F. P. 2007, ApJ, 666, 1152

Dib, R., Kaspi, V. M., & Gavriil, F. P. 2008a, ApJ, 673, 1044

Dib, R., Kaspi, V. M., & Gavriil, F. P. 2008b, in American Institute of Physics Conference Series, Vol. 983, 40 Years of Pulsars: Millisecond Pulsars, Magnetars and More, 239–243

—. 2009a, ApJ, 702, 614

Dib, R., Kaspi, V. M., & Gavriil, F. P. 2009b, in Thirty Years of Magnetars: New Frontiers, ed. S. Zane, R. Turolla, G. Israel, & C. Kouveliotou, Aspen Winter Conference on Astrophysics

Dierckx, F. 1975, J. Comput. Appl. Math., 1, 165

Ertan, Ü., Ekşi, K. Y., Erkut, M. H., & Alpar, M. A. 2009, ApJ, 702, 1309

Espinoza, C. M., Lyne, A. G., Kramer, M., Manchester, R. N., & Kaspi, V. M. 2011, ApJ, 741, L13

Fahlman, G. G. & Gregory, P. C. 1981, Nature, 293, 202

Gavriil, F. P., Dib, R., & Kaspi, V. M. 2011, ApJ, 736, 138

Gavriil, F. P., Gonzalez, M. E., Gotthelf, E. V., Kaspi, V. M., Livingstone, M. A., & Woods, P. M. 2008, Science, 319, 1802

Gavriil, F. P. & Kaspi, V. M. 2002, ApJ, 567, 1067

—. 2004, ApJ, 609, L67

Gavriil, F. P., Kaspi, V. M., & Woods, P. M. 2002, Nature, 419, 142

—. 2004, ApJ, 607, 959

Gavriil, F. P., Kaspi, V. M., & Woods, P. M. 2006, ApJ, 641, 418

Gonzalez, M. E., Dib, R., Kaspi, V. M., Woods, P. M., Tam, C. R., & Gavriil, F. P. 2010, ApJ, 716, 1345

Halpern, J. P. & Gotthelf, E. V. 2005, ApJ, 618, 874

Helfand, D. J., Gotthelf, E. V., & Halpern, J. P. 2001, ApJ, 556, 380

Hurley, K., Li, P., Kouveliotou, C., Murakami, T., Ando, M., Strohmayer, T., van Paradijs, J., Vrba, F., Luginbuhl, C., Yoshida, A., & Smith, I. 1999, ApJ, 510, L111

Içdem, B., Baykal, A., & Inam, S. Ç. 2012, MNRAS, 419, 3109

Israel, G. L., Esposito, P., Rea, N., Dall'Osso, S., Senziani, F., Romano, P., Mangano, V., Götz, D., Zane, S., Tiengo, A., Palmer, D. M., Krimm, H., Gehrels, N., Mereghetti, S., Stella, L., Turolla, R., Campana, S., Perna, R., Angelini, L., & de Luca, A. 2010, MNRAS, 408, 1387

Israel, G. L., Götz, D., Zane, S., Dall'Osso, S., Rea, N., & Stella, L. 2007, A&A, 476, L9

Iwasawa, K., Koyama, K., & Halpern, J. P. 1992, PASJ, 44, 9

Jahoda, K., Swank, J. H., Giles, A. B., Stark, M. J., Strohmayer, T., Zhang, W., & Morgan, E. H. 1996, Proc. SPIE, 2808, 59

Kaspi, V. M., Chakrabarty, D., & Steinberger, J. 1999, ApJ, 525, L33

Kaspi, V. M. & Gavriil, F. P. 2003, ApJ, 596, L71

Kaspi, V. M., Gavriil, F. P., Chakrabarty, D., Lackey, J. R., & Muno, M. P. 2001, ApJ, 558, 253

Kaspi, V. M., Gavriil, F. P., Woods, P. M., Jensen, J. B., Roberts, M. S. E., & Chakrabarty, D. 2003, ApJ, 588, L93

Kaspi, V. M., Lackey, J. R., & Chakrabarty, D. 2000, ApJ, 537, L31

Kouveliotou, C., Dieters, S., Strohmayer, T., van Paradijs, J., Fishman, G. J., Meegan, C. A., Hurley, K., Kommers, J., Smith, I., Frail, D., & Murakami, T. 1998, Nature, 393, 235

Kouveliotou, C., Strohmayer, T., Hurley, K., Van Paradijs, J., Finger, M. H., Dieters, S., Woods, P., Thompson, C., & Duncan, R. C. 1999, ApJ, 510, L115

Kulkarni, S. R., Kaplan, D. L., Marshall, H. L., Frail, D. A., Murakami, T., & Yonetoku, D. 2003, ApJ, 585, 948

Lin, L., Kouveliotou, C., Göğüş, E., van der Horst, A. J., Watts, A. L., Baring, M. G., Kaneko, Y., Wijers, R. A. M. J., Woods, P. M., Barthelmy, S., Burgess, J. M., Chaplin, V., Gehrels, N., Goldstein, A., Granot, J., Guiriec, S., Mcenery, J., Preece, R. D., Tierney, D., van der Klis, M., von Kienlin, A., & Zhang, S. N. 2011, ApJ, 740, L16

Livingstone, M. A., Kaspi, V. M., Gotthelf, E. V., & Kuiper, L. 2006, ApJ, 647, 1286

Mazets, E. P., Golenetskii, S. V., Ilinskii, V. N., Apetkar, R. L., & Guryan, Y. A. 1979, Nature, 282, 587

Mereghetti, S. 1995, ApJ, 455, 598

Mereghetti, S., Israel, G. L., & Stella, L. 1998, MNRAS, 296, 689

Mereghetti, S. & Stella, L. 1995, ApJ, 442, L17

Morii, M., Kawai, N., & Shibazaki, N. 2005, ApJ, 622, 544

Olausen, S. & Kaspi, V. M. 2013, ApJ Supplement Series, in prep.

Paul, B., Kawasaki, M., Dotani, T., & Nagase, F. 2000, ApJ, 537, 319

Perna, R. & Pons, J. A. 2011, ApJ, 727, L51

Pines, D. & Alpar, M. A. 1985, Nature, 316, 27

Pons, J. A. & Perna, R. 2011, ApJ, 741, 123

Rea, N., Oosterbroek, T., Zane, S., Turolla, R., Méndez, M., Israel, G. L., Stella, L., & Haberl, F. 2005, MNRAS, 361, 710

Scholz, P., Ng, C.-Y., Livingstone, M. A., Kaspi, V. M., Cumming, A., & Archibald, R. F. 2012, ApJ, 761, 66

Sugizaki, M., Nagase, F., Torii, K. I., Kinugasa, K., Asanuma, T., Matsuzaki, K., Koyama, K., & Yamauchi, S. 1997, PASJ, 49, L25

Tam, C. R., Gavriil, F. P., Dib, R., Kaspi, V. M., Woods, P. M., & Bassa, C. 2008, ApJ, 677, 503

Thompson, C. & Duncan, R. C. 1993, ApJ, 408, 194

Thompson, C. & Duncan, R. C. 1995, MNRAS, 275, 255

Thompson, C. & Duncan, R. C. 1996, ApJ, 473, 322

Thompson, C., Lyutikov, M., & Kulkarni, S. R. 2002, ApJ, 574, 332

Tiengo, A., Mereghetti, S., Turolla, R., Zane, S., Rea, N., Stella, L., & Israel, G. L. 2005, A&A, 437, 997

van Paradijs, J., Taam, R. E., & van den Heuvel, E. P. J. 1995, A&A, 299, L41

Vasisht, G. & Gotthelf, E. V. 1997, ApJ, 486, L129

Weltevrede, P., Johnston, S., & Espinoza, C. M. 2011, MNRAS, 411, 1917

Woods, P. M., Kaspi, V. M., Thompson, C., Gavriil, F. P., Marshall, H. L., Chakrabarty, D., Flanagan, K., Heyl, J., & Hernquist, L. 2004, ApJ, 605, 378

Yu, M., Manchester, R. N., Hobbs, G., Johnston, S., Kaspi, V. M., Keith, M., Lyne, A. G., Qiao, G. J., Ravi, V., Sarkissian, J. M., Shannon, R., & Xu, R. X. 2013, MNRAS, 429, 688

Zhu, W. & Kaspi, V. M. 2010, ApJ, 719, 351

Zhu, W., Kaspi, V. M., Dib, R., Woods, P. M., Gavriil, F. P., & Archibald, A. M. 2008, ApJ, 686, 520

This 2-column preprint was prepared with the AAS LaTeX macros v5.2.